Chemical Engineering Journal 460 (2023) 141795

Contents lists available at ScienceDirect

Chemical Engineering Journal

journal homepage: www.elsevier.com/locate/cej

# Highly scalable acid-base resistant Cu-Prussian blue metal-organic framework for $C_2H_2/C_2H_4$, biogas, and flue gas separations

Shyam Chand Pal [a], Rajamani Krishna [b,*], Madhab C. Das [a,*]

[a] Department of Chemistry, Indian Institute of Technology Kharagpur, Kharagpur 721302, WB, India
[b] Van 't Hoff Institute for Molecular Sciences, University of Amsterdam, Science Park 904, 1098 XH Amsterdam, The Netherlands

ARTICLE INFO

*Keywords:*
Prussian blue
Metal-organic framework (MOF)
pH stable MOF
Gas Separation
Biogas
Flue gas

ABSTRACT

One of the emerging problems plaguing the chemical industry today is the selective capture and separation of gases from their mixtures in an efficient and cost-effective manner. MOFs are new-age physisorbent materials extensively investigated for various gas mixture separations (such as biogas, flue gas, olefin/paraffin *etc.*); however, face the challenge of separations in a realistic environment. Here, we have investigated one of the Prussian blue analogues (Cu-PSB) to explore its potential as energy-efficient gas separation material. Cu-PSB can easily be scaled up at room temperature from water and is highly robust under harsh acidic, basic environments (pH = 1–11, 6 M HCl, 18 M $H_2SO_4$), exhibiting excellent separation of $C_2H_2/C_2H_4$, biogas ($CO_2$:$CH_4$ = 50:50), and flue gas ($CO_2$:$N_2$ = 15:85) mixtures. The IAST selectivity at ambient conditions (295 K, 50:50 mixture) could reach up to 5.2 for $C_2H_2/C_2H_4$, 14.7 for $CO_2/CH_4$, and 60.5 for the $CO_2/N_2$ (15:85 mixture). Such high $C_2H_2$ and $CO_2$ uptake capacity and separation selectivity could be attributed to the synergistic effect of open $Cu^{II}$ sites and the multiple H-bonding interactions within the functional pore channels of optimal pore size. Further, breakthrough simulation confirmed the complete separations from their binary mixtures, thus proving to be highly useful for the $C_2H_2/C_2H_4$ separation and $CO_2$ capture from the bio and post-combustion flue gas mixtures. Cu-PSB was found to be even a more robust framework than ZIF-8 and UiO-66 MOFs.

## 1. Introduction

In the past decade, classical porous materials, such as zeolites, silica, and activated carbon molecular sieves, have been extensively investigated as adsorbents for capturing and/or separating $CO_2$ and lighter hydrocarbon mixtures as an alternative technology to traditional energy-intensive amine absorption and cryogenic distillation processes [1–3]. By comparison, the physisorbent could offer much-reduced energy footprints for the efficient separation and purification of gas mixtures [4,5]. Thus, much effort has been devoted in exploring the physisorbent materials with precisely controllable structures and tunable chemical pore environments for the targeted gas separations. In particular, the versatile functionality and high structural tunability through the modulation of the building units in Metal-organic frameworks (MOFs) render these materials to serve as promising adsorbent/separation materials in recent decades for different gas mixtures [6–21]. Generally, the gas mixture separations in MOFs can be divided into two broad categories non-equilibrium and equilibrium types [6]. The former cases mainly involve kinetic separation and molecular sieving through fine-tuning the pore window and the framework's flexibility [6]. Although material that can selectively sieving out a particular gas molecule from a mixture while maintaining high adsorption capacity is highly desirable for practical application, they are scarce in the literature [6,7]. In the latter case, the thermodynamic affinity difference between the host and the guest plays a crucial role in the separation process which can be further controlled through pore wall functionalization by installing targeted functional groups (–$NH_2$, –OH, -F etc.) and/or incorporating open metal sites [6,8,10]. The well-known MOF-74 family bearing high-density of open metal sites could enhance high adsorption capacity, however, suffers from poor stability under moisture-containing environments [22,23]. Recently, the SIFSIX family has shown great promise in balancing the high adsorption capacity and selectivity. Although, the grand challenge of high adsorption capacity and selectivity with lower regeneration energy has significantly been improved through preferential binding of $C_2H_2$ molecules in SIFSIX materials by cooperative host − guest and/or guest − guest interactions [24], in general, the poor stability of these anion-pillared hybrid porous materials limits their practical implementation under industrial

* Corresponding authors.
*E-mail addresses:* r.krishna@contact.uva.nl (R. Krishna), mcdas@chem.iitkgp.ac.in (M.C. Das).

https://doi.org/10.1016/j.cej.2023.141795
Received 8 December 2022; Received in revised form 25 January 2023; Accepted 6 February 2023
Available online 10 February 2023

conditions (high RH and ppm of $SO_2$, and $NO_2$) [25–27]. Also, the organic linker used to construct those MOFs is costly; subsequently, the production cost of MOFs is also high, making them hardly economical for large-scale industrial applications [28]. Having said that in-general highly porous MOFs adsorbents are expensive because of costly organic linkers coupled with tedious synthesis processes and usage of non-aqueous solvents together with solvothermal set up and overall the practical concern of poor hydrolytic stability (most of the classical MOFs are prone to degrade in water), the development of highly scalable MOFs through cost-effective easily available struts through simple room temperature crystallization from aqueous medium could pave the way for their plausible industrialization. Such simple crystallization has already been adopted in industry to produce a large number of chemicals at the required scales [5]. Therefore, significant efforts are required to develop highly scalable robust MOFs with high chemical stability (water and pH), excellent selectivity, and targeted uptake capacity with easy regenerability for cost-effective industrially relevant gas mixture separations.

Ethylene ($C_2H_4$) is a key feedstock in the chemical and petrochemical industry, containing traces amount of acetylene ($C_2H_2$) as an impurity during the cracking of heavier hydrocarbons [29]. The trace $C_2H_2$ can poison Ziegler–Natta catalysts and lower the quality of the end product obtained from $C_2H_4$ polymerization. Thus trace $C_2H_2$ should be removed to extremely low thresholds (less than 40 ppm) to protect the catalyst from poisoning [29]. Meanwhile, $C_2H_2$ is used as fuel and an important building block for several other derivatives [30]. Notably, the elimination of $C_2H_2$ from $C_2H_4$ is one of the most demanding tasks due to the similar physical properties (molecular sizes: 3.32 × 3.34 × 5.70 $Å^3$ for $C_2H_2$ versus 3.28 × 4.18 × 4.84 $Å^3$ for $C_2H_4$) which consumes a considerable amount of energy through the traditional distillation process [4]. On the other hand, $CO_2$ is a greenhouse gas, and its capture and separations from localized emission sources and several industrially relevant gas mixtures are essential industrial processes [31]. Flue gas from coal-fired power plants, a primary $CO_2$ emission source, contains 13–15 % of $CO_2$ diluted mostly with $N_2$, water (8–10 %), and acidic gases [31]. On the other hand, biogas is a source of bio-methane, which contains a variable amount of $CO_2$, and thus requires the removal of $CO_2$ and other impurities [31]. The capture of $CO_2$ from these sources allows it to produce a range of chemicals, products, and materials that minimize the effects of $CO_2$ emission into the atmosphere [31]. The currently used bio and flue gas separation techniques are energy-intensive cryogenic distillations and amine-based chemisorbents [32]. Although chemisorbents are effective in $CO_2$ removal, they typically require high regeneration energy of about 30 % of the output of the power plants, and chemical decomposition often takes place [32]. Thus, the demand for energy-saving methods such as non-thermal physical adsorption using porous adsorbents for the purifications of $C_2H_4$ from $C_2H_2$ and capturing of $CO_2$ from bio and flue gas mixtures has driven a significant development of adsorption-based technology as it can offer a potential solution to the selectively capture and more facile regeneration.

Prussian blue (PSB) is one of the oldest compounds, arguably the first one, reported in the history of coordination chemistry, a well-known Hofmann-type compound composed of a very short cyanide ligand [33]. PSB analogues have been explored for diverse applications, including gas storage [34,35], energy storage [36], electrocatalysis [37], and spin-crossover materials [38]. Like the aromatic linker in MOFs, the cyanide bridges in these materials create well-defined microporous channels decorated with polarizable $\pi$-electron that are expected to have different affinities for guest molecules [33]. Moreover, PSB analogues possess open coordination sites on the $M^{II}$ arising upon removing the bound water molecules, which may selectively interact with the guest molecules. Here, we have selected an ultra-microporous Cu-PSB to investigate its $C_2H_2/C_2H_4$, $CO_2/CH_4$, and $CO_2/N_2$ gas separation performance under ambient conditions, as these separations are yet to be explored with these types of frameworks [33]. Although the $N_2$ and $H_2$ adsorption properties could be found in the literature with the dehydrated Prussian blue analogues of the type $M_3[Co(CN)_6]_2$, their gas separations remain unexplored till date [33–35]. Single-component gas adsorption experiments revealed a high $C_2H_2$ and $CO_2$ uptake of 79.9, and 84 $cm^3\ g^{-1}$ at 295 K under 1 bar and an excellent selectivity of 4.5, and 5.2 (1:99 and 50:50 mixture of $C_2H_2/C_2H_4$), 14.7 for $CO_2/CH_4$ (50:50), and 60.5 for the $CO_2/N_2$ (15:85 mixture) with moderate heat of adsorption for $C_2H_2$ (20–42 kJ $mol^{-1}$) and $CO_2$ (19 kJ $mol^{-1}$) compared to the benchmark MOFs. The optimal pore size in Cu-PSB and the functional pore channels containing the cyanide ligands and open $Cu^{II}$ sites could collaboratively enforce the stronger interaction (H-bonding with cyanide ligands and electrostatic interaction with open $Cu^{II}$ sites) with the acidic $C_2H_2$ and $CO_2$ molecules. Thus high separation selectivity for the $C_2H_2/C_2H_4$ mixture, and high uptake capacity of $CO_2$ from bio, and post-combustion flue gas mixture under ambient conditions could be achieved as evident from transient breakthrough simulations. Our findings show that Cu-PSB is highly scalable through simple room temperature crystallization from water and highly robust under harsh acidic, basic environments (pH = 1–11). Cu-PSB was found to be even a more robust framework than ZIF-8 and UiO-66.

## 2. Results and Discussion:

Cu-PSB was easily scaled up as fine crystalline powder by mixing Cu (II) salt with $K_3[Co(CN)_6]$ in water under ambient conditions [34,35]. Cu-PSB possesses a simple three-dimensional cubic (α-Po) structure type consisting of open $Cu^{II}$ sites due to the vacancies at $[Co(CN)_6]^{3-}$ sites within the cubic framework (Fig. 1). The coordinated and guest water molecules inside the pores located in crystallographically distinct positions fill these $Cu^{II}$ surrounding vacancies and can be removed without destroying the framework (Fig. 1b, c). X-ray powder diffraction patterns (PXRD) of the microcrystalline powder of Cu-PSB were fully consistent with the usual PSB structure type and showed sharp, intense peaks (Figure S1). The resultant Cu-PSB was further validated by elemental analysis, thermogravimetric analysis (TGA), and FT-IR analysis (Figures S2 and S3). The chemical composition of Cu-PSB has been confirmed from the TGA and elemental analysis, indicating the presence of less than 0.1 equivalent potassium per formula unit (Figure S4).

Furthermore, bulk samples of PSB can be easily scaled up in gram scale from commercially available and inexpensive reagents using a fast and direct mixing in water at room temperature, as inferred from the PXRD (Figure S5). The solvent stability in different laboratory organic solvent (DMF, DMA, $CHCl_3$, MeOH, EtOH, THF, and ACN) checked for 7 days, suggesting good chemical stability (Figure S6). The fast and facile synthesis method at room temperature from a green aqueous medium, excellent chemical stability (discussed in a subsequent section), and the microporous nature indicates the promise of Cu-PSB as a gas separation material.

The well-dried sample of Cu-PSB was activated under a dynamic vacuum at 100 °C for 24 h before the gas adsorption measurements. The structural stability after activation was further confirmed from powder X-ray diffraction, and a consistent pattern with the as-synthesized Cu-PSB was noticed (Figure S7). The permanent microporosity in Cu-PSB was determined from the $N_2$ adsorption isotherm at 77 K as depicted in Fig. 2a. The BET surface area (Langmuir) was calculated to be 651 (1003) $m^2\ g^{-1}$ and the total pore volume of 0.30 $cm^3\ g^{-1}$ (Figure S8).

The one-dimensional channels with a suitable window size of (~4.4 × 4.4 $Å^2$) decorated with polarizable π-electron clouds of the cyanide bridges and the presence of unsaturated $Cu^{II}$ sites are expected to show different interactions with the guest molecules (Fig. 1b, c). The single-component gas adsorption of $C_2H_2$, $C_2H_4$, $CO_2$, $CH_4$, and $N_2$ were thus measured at 273 and 295 K up to 1 bar pressure (Fig. 2b, c). It is to be noted that the adsorption and desorption points at both temperatures almost coincide with each other indicating reversible sorption processes. As depicted in Fig. 2b, and c, Cu-PSB exhibited a sharp uptake for $C_2H_2$, at both temperatures reaching a value of 97 (4.33 mmol $g^{-1}$), and 79 (3.52 mmol $g^{-1}$), $cm^3\ g^{-1}$, whereas for the $C_2H_4$ the uptakes were 61

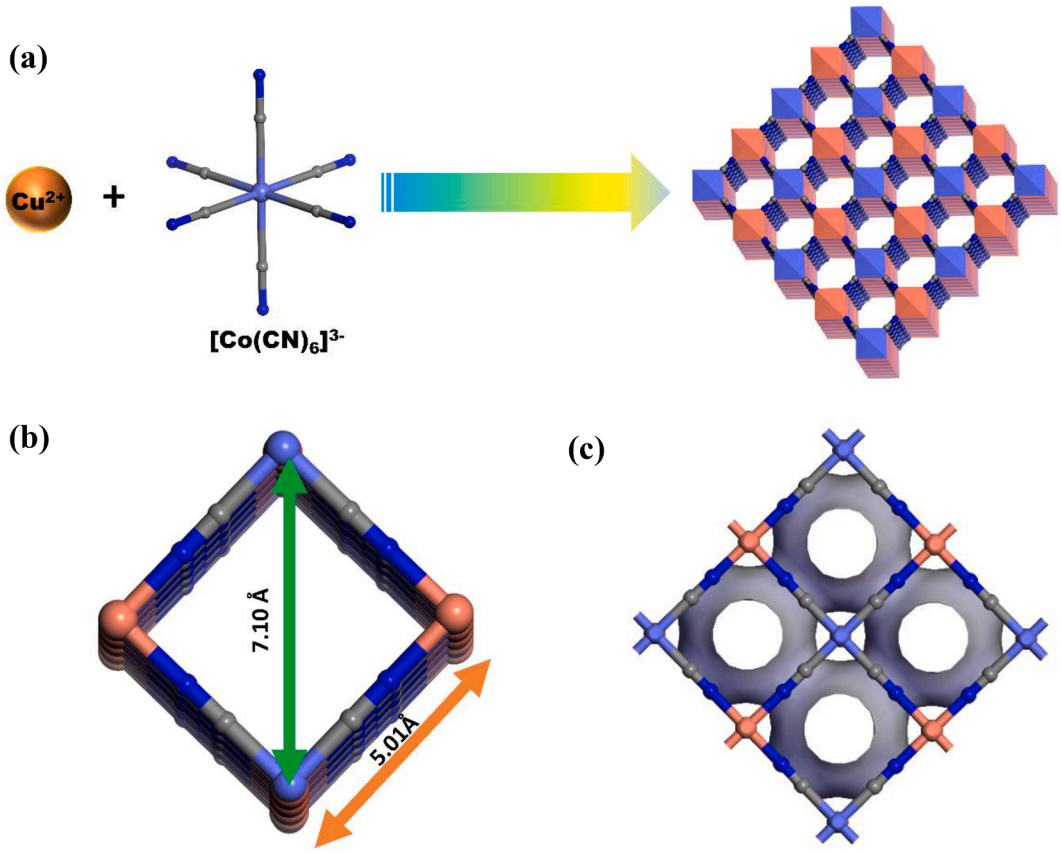


**Fig. 1.** Structural representation of Cu-PSB. (a) Individual precursor and the three-dimensional network structure. (b) A portion of Cu-PSB showing the single pore channel with the distance between the two oppositely metal centers. (c) Pore window of (~4.4 × 4.4 Å$^2$) along the crystallographic '*a*' axis. Color code, Dark orange, Cu; light blue, Co; grey, C; and royal blue, N. (For interpretation of the references to color in this figure legend, the reader is referred to the web version of this article.)

(2.72 mmol g$^{-1}$), and 53 (2.36 mmol g$^{-1}$), at 273 and 295 K respectively under 1 bar pressure. Such high $C_2H_2$ uptake of Cu-PSB at 295 K is comparable to the other Hofmann-type frameworks, such as ZJU-74 (3.82 mmol g$^{-1}$) [39], FeNi-M′MOF (4.29 mmol g$^{-1}$) [40] and Cu(bpy)NP (2.26 mmol g$^{-1}$) [41] and some of the benchmark MOF adsorbents, UTSA-200a (3.65 mmol g$^{-1}$) [25], SIFSIX-2-Cu-I (4.02 mmol g$^{-1}$) [24] SOFOUR-1-Zn (3.1 mmol g$^{-1}$) [42], ZNU-1 (3.4 mmol g$^{-1}$) [43], [Ni$_2$(L-mal)$_2$(bpy)] (3.04 mmol g$^{-1}$) [44], BSF-3 (3.56 mmol g$^{-1}$) [45] JCM-1 (3.55 mmol g$^{-1}$) (Table S1) [46]. Further, the uptake ratio of $C_2H_2/C_2H_4$ for the Cu-PSB was compared with those reported MOFs having the separation performance solely rely on the thermodynamic affinity between the host and guest (Fig. 2d). The high $C_2H_2/C_2H_4$ uptake ratio of 1.49 is similar to the well-known high performing MOF based adsorbents relying on the thermodynamic separation such as Mg-MOF-74 (1.12) [22,23], NOTT − 300 (1.48) [47], CPL-5 (1.64) [48], SIFSIX-2-Cu-i (1.84) [24], UTSA-100a (2.57) [49].

On the other hand, Cu-PSB also exhibited selective uptake of $CO_2$, with respect to $CH_4$ and $N_2$, and the corresponding uptake values are 108 (4.82 mmol g$^{-1}$), 24 (1.07 mmol g$^{-1}$), and 7.5 (0.33 mmol g$^{-1}$) cm$^3$ g$^{-1}$ at 273 K and 84 (3.75 mmol g$^{-1}$) 18 (0.80 mmol g$^{-1}$), 4.9 (0.21 mmol g$^{-1}$) cm$^3$ g$^{-1}$ at 295 K (Fig. 2b, Table S2). The low-pressure $CO_2$ adsorption (0.15 bar) is an important parameter to determine the potential of flue gas separation of any material. Cu-PSB exhibits high $CO_2$ uptake of 1.25 mmol at 295 K (0.15 bar), similar to SIFSIX-14-Cu-I (1.42 mmol) and higher than Qc-5-Cu-sql (0.73 mmol) [50,51]. Moreover, $CO_2$ uptake at 1 bar is comparable to many well-known MOFs such as MFM-130 (109 cm$^3$/g at 273 K and 59 cm$^3$/g at 298 K) [52], MAF-23 (74.2 cm$^3$/g at 273 K and 56.1 cm$^3$/g at 298 K) [53], ZIF-69 (70 cm$^3$/g at 273 K) [54], and BIF-41 (77.0 cm$^3$/g at 273 K and 63.5 cm$^3$/g at 294 K) [55].

The difference in uptake values of these gas molecules by Cu-PSB was validated by the isosteric heat of adsorption ($Q_{st}$) calculated from the single component adsorption isotherm collected at different temperatures (Fig. 2e). The $Q_{st}$ value for $C_2H_2$ is in the range of 20–42 kJ mol$^{-1}$, whereas, for $C_2H_4$, the value is 6.4–23 kJ mol$^{-1}$. Interestingly, at near-zero coverage, $Q_{st}$ values for $C_2H_4$ are significantly lower than $C_2H_2$. However, with the increasing loading of the gas molecules, the $Q_{st}$ value for both $C_2H_2$ and $C_2H_4$ increases and reaches a maximum at equilibrium, suggesting a cooperative interaction between the guests. The maximum $Q_{st}$ value for $C_2H_2$ (42 kJ mol$^{-1}$) is lower than NKMOF-1-Ni (60.3 kJ mol$^{-1}$) [56], and ZJU-74 (45–65 kJ mol$^{-1}$) [39] with a high density of OMSs, however comparable with Cu(bpy)NP (40.8 kJ mol$^{-1}$) [41], and FeNi-M′MOF (27–32.8 kJ mol$^{-1}$) [40] (Fig. 2f and Table S1). As expected from the uptake capacity, the $Q_{st}$ values for $CO_2$, $CH_4$, and $N_2$ are 19, 11.8, and 13 kJ mol$^{-1}$ and remain almost unchanged in the whole pressure range. Noticeably, the $Q_{st}$ value for $CO_2$ is significantly lower, thus suggesting facile and cost-effective regeneration.

The significant uptake difference obtained from single component adsorption data between $C_2H_2$ and $C_2H_4$ in **Cu-PSB** motivated us to explore the separations of $C_2H_2/C_2H_4$ (1:99 and 50:50), because of their practical relevance, as discussed in the introduction section. The dual-site Langmuir model was employed to fit the single-component gas sorption data measured at different temperatures, and the corresponding fitting parameters (Table S3) were used for selectivity calculation through the IAST method. The IAST selectivity of **Cu-PSB** toward $C_2H_2/C_2H_4$ mixture is 9.4 and 14.3 at 273 K, (Figures S9 and S10) whereas these values at 295 K are 4.5 and 5.2 for the 1:99 and 50:50 mixture (Fig. 3a and 3b) respectively. The selectivity values at 295 K are

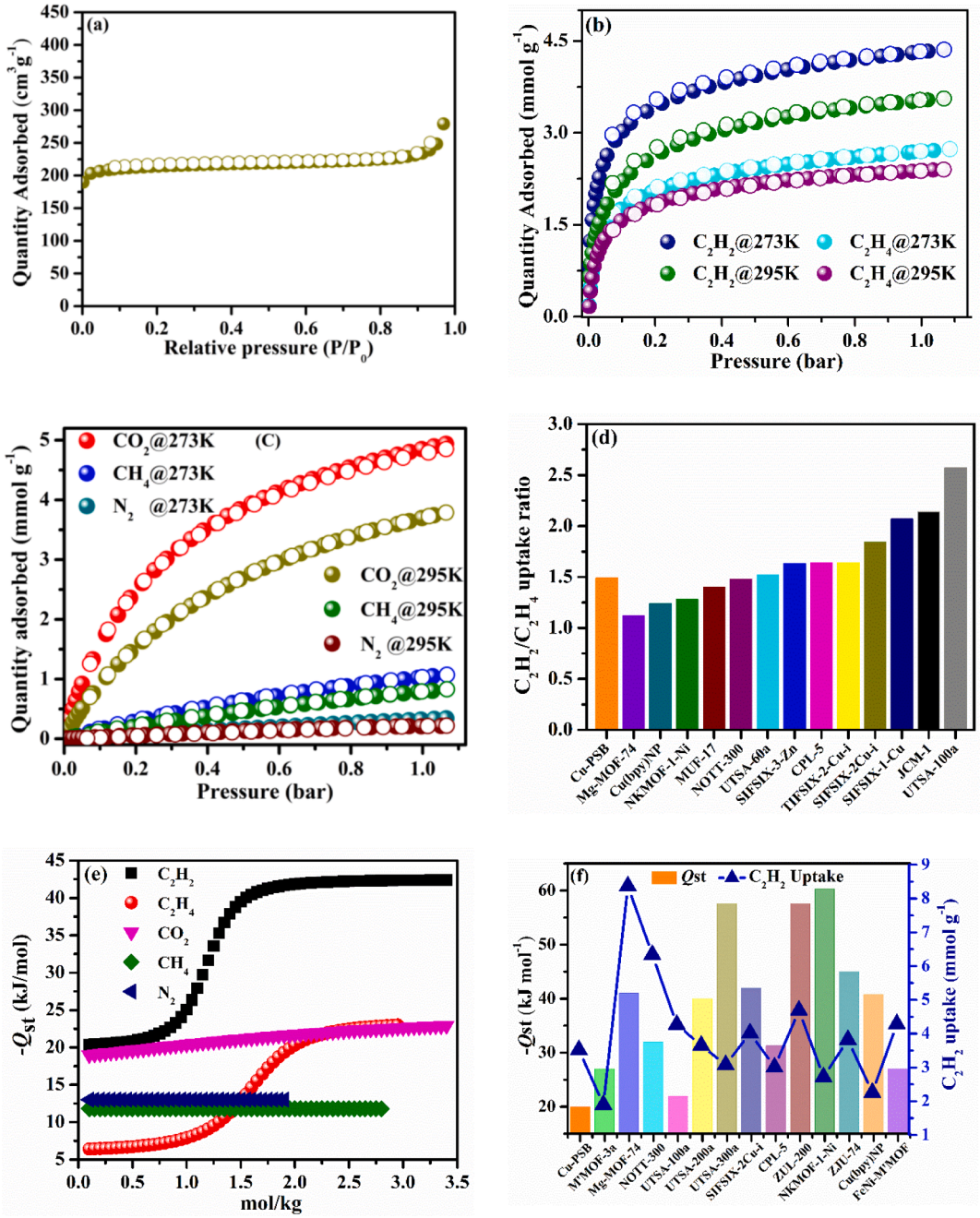


**Fig. 2.** Gas adsorption performance of Cu-PSB. (a) $N_2$ adsorption isotherm at 77 K. (b) $C_2H_2$ and $C_2H_4$; (c) $CO_2$, $CH_4$, and $N_2$ sorption isotherms at different temperatures. (d) $C_2H_2/C_2H_4$ uptake ratio comparison of Cu-PSB with some of best performing $C_2H_2/C_2H_4$ separating MOFs. (e) $Q_{st}$ of different gases for Cu-PSB. (f) Comparison of $Q_{st}$ and $C_2H_2$ uptake with some well-known MOFs ($Q_{st}$ in bar diagram, $C_2H_2$ uptakes in blue triangle). The filled and open circles represent the adsorption and desorption points. (For interpretation of the references to color in this figure legend, the reader is referred to the web version of this article.)

comparable (Table S1) to some of the well-known literature reports based on thermodynamic separation, such as SIFSIX-1-Cu (7.1 to 10.6; 1:99) [24], CPL-5 (5.99; 1:99) [48], FeMOF-74 (2.1; 1:99) [22] and NOTT-300 (2.2 to 2.5; 1:99) [47], SIFSIX-3-Zn (8.8; 1:99) [24] and SIFSIX-3-Ni (5.0; 1:99) [24], MUF-17 (7; 1:99) [57], UTSA-100a (10; 1:99) [49] and lower than Cu(bpy)NP (28.5;1:99) [41] (Fig. 3e). Similarly for the equimolar $C_2H_2/C_2H_4$ selectivity at 295 K is comparable to Fe-MOF-74 (1.87) [22], M′MOF-2a (1.93) [58], NOTT-300 (2.3) [47], but lower than that of SIFSIX-2-Cu-I (41.01) [24].

Besides excellent $C_2H_2/C_2H_4$ separation selectivity, Cu-PSB exhibited excellent biogas ($CO_2$:$CH_4$ = 50:50) and flue gas ($CO_2$:$N_2$ = 15:85) separation performance (Fig. 3c-3d and Figures S11-S12). The corresponding IAST selectivity values for the biogas are 26.5 (273 K) and 14.7 (295 K), which is higher than many well-known MOFs (Table S4) such as HKUST-1(7.5) [59], MIL-53(Al) (2.3) [60], SIFSIX-2-Cu (5.3) [61] ZIF-100 (5.9) [62] IITKGP-12 (12) [63] and Zeolite 13X (3.6) [64] (Fig. 3f). For the flue gas mixture, the separation selectivity values are 95.2 (273 K) and 60.5 (295 K), respectively (Table S4). The IAST separation selectivity is comparable to LIFM-11 (68.9 at 298 K) [65] and is higher than UTSA-72 (35.6) [66], PCN-88 (15.2) [67], and BUT-11 (31.5) [68] at 298 K (Fig. 3f, and Table S4) and thus suggesting the prospective of Cu-PSB toward such important gas separations.

It is well known that PSB analogues possess open coordination sites on the $M^{II}$ arising upon removing the bound water molecules [33–35]. The high separation selectivity of Cu-PSB toward the $C_2H_2/C_2H_4$ mixture could be attributed to the presence of strong host–guest

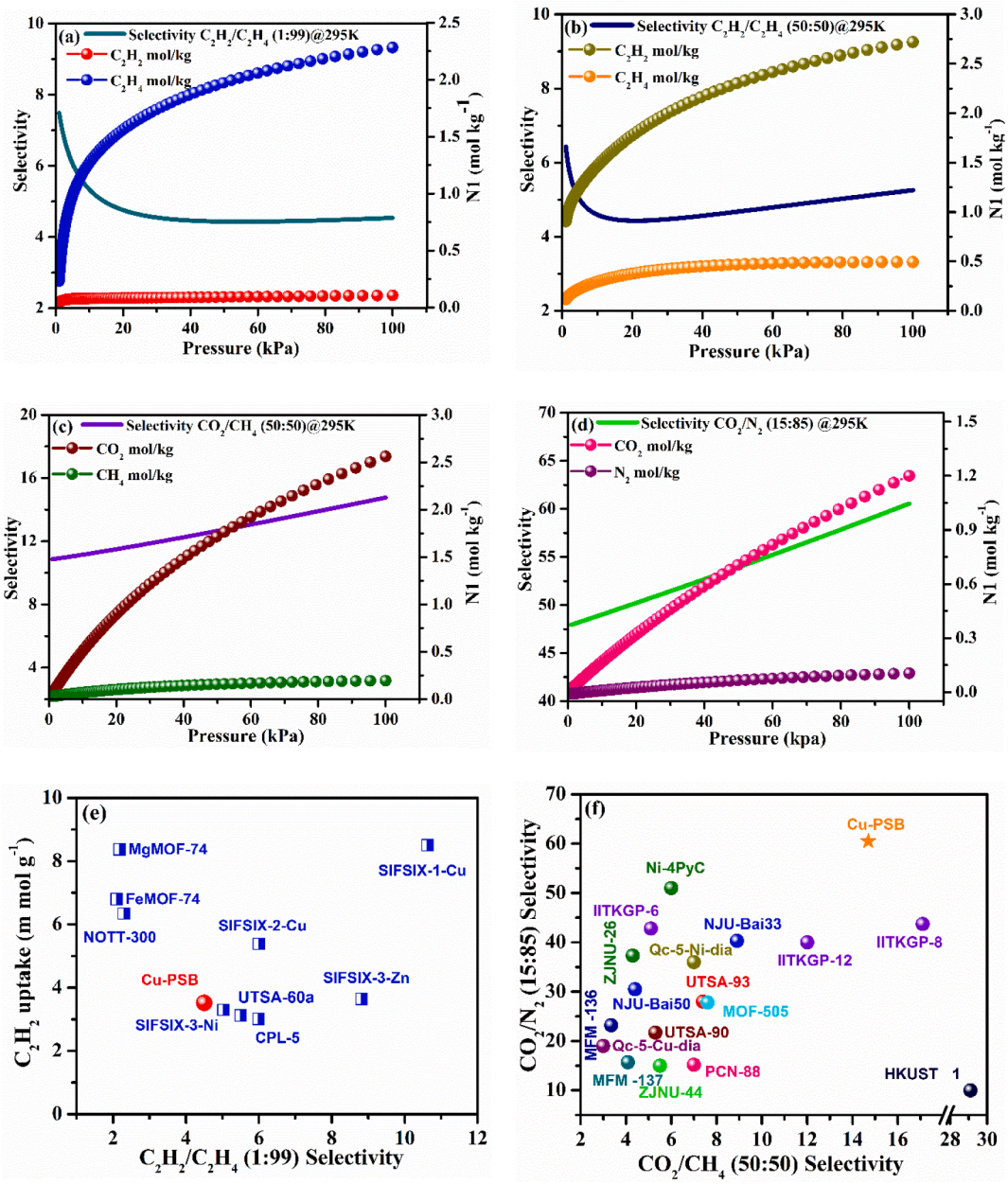


**Fig. 3.** Predicted IAST selectivity and mixed gas isotherm of Cu-PSB at 295 K for (a) $C_2H_2/C_2H_4$ (1:99) (b) $C_2H_2/C_2H_4$ (50:50) (c) $CO_2$ /$CH_4$ (50:50) and $CO_2$ /$N_2$ (15:85) mixture. (e) Comparison of $C_2H_2$ uptake and $C_2H_2$/ $C_2H_4$ IAST adsorption selectivity of Cu-PSB with other porous MOFs at 295 K under 1 bar. (f) Comparison of IAST adsorption selectivity of $CO_2/CH_4$ and $CO_2/CH_4$ of Cu-PSB with MOF materials at 295 K under 1 bar.

interactions with the OMSs as well as multiple weak hydrogen bonding interactions within the functional pore channels containing the polarizable π electron cloud of the cyanide building block (Fig. 1b and c). Although $C_2H_2$ and $C_2H_4$ could get inside the pores because of the very similar empirical kinetic diameters, $C_2H_2$ is better able to interact with the unsaturated metal centers electrostatically due to higher acidity (*p*Ka values of $C_2H_2$, 25, and $C_2H_4$, 44) thus enforce the high $C_2H_2$ uptake and selectivity. In contrast, such interactions were weak for the $C_2H_4$ molecules. Further, $C_2H_2$ molecules are densely packed within the pores through cooperative interaction, as can be seen from the $Q_{st}$ value, which increases with increasing the loading ($C_2H_2$, 20–42 kJ $mol^{-1}$). Although such type of cooperative behaviour for $CO_2$ was not observed, $CO_2$ possesses quadruple moments through which it can strongly binds with the polar channels and open metal sites. $CH_4$ and $N_2$ do not possess any such type of quadruple moments and thus exhibited the lowest $Q_{st}$ among the others.

Apart from separation selectivity, the quantity of uptake of any adsorbent from the mixed phase is another determining factor in a pressure swing adsorption (PSA) unit for its practical deployment in industrial gas separations [69]. Thus, we have determined the $C_2H_2$ and $CO_2$ loading within the porous structure for the mixtures of $C_2H_2/C_2H_4$ (1:99 & 50:50) $CO_2/CH_4$ (50:50), and $CO_2/N_2$ (15:85) at 273 and 295 K under 100 kPa pressure using IAST method. As shown in Fig. 3b and Figure S10, $C_2H_2$ loadings from the simulated binary gas mixtures ($C_2H_2/C_2H_4$ = 50:50) at 273 and 295 K under 100 kPa are considerably higher compared to the $C_2H_4$. The corresponding uptake values of $C_2H_2$ are 3.62 and 2.72 mol $kg^{-1}$ at 273 and 295 K (Fig. 3b and Figure S10), respectively. The captured amount of $CO_2$ from simulated $CO_2/CH_4$ (50:50 mixture) is 3.65 (273 K) and 2.56 (295 K) mol $kg^{-1}$, and for the $CO_2/N_2$ (15:85) mixture, 1.94 (273 K) and 1.20 (295 K) mol $kg^{-1}$ (Fig. 3c and 3d), which is similar to the previously observed MOFs [63,70,71].

In PSA unit, the potential of the physisorbent is determined from the selectivity and uptake capacity which can be obtained from the breakthrough analysis [69]. Transient breakthrough thus has been performed to check further the feasibility of Cu-PSB for the following gas mixtures separations $C_2H_2/C_2H_4$ (1:99 and 50:50), $CO_2/CH_4$ (50:50), and $CO_2/N_2$ (50:50) at temperatures of 273 K and 295 K (Fig. 4 and Figures S13-S16). Fig. 4a and 4b revealed the dimensionless concentrations of $C_2H_2/C_2H_4$ exiting the adsorbed packed with Cu-PSB as a function of the corrected time ($Q_0$ t/$m_{ads}$), at 1 bar and 295 K. Complete separation could be accomplished by Cu-PSB, whereby $C_2H_4$ breakthrough occurred first. The corresponding productivity of polymer-grade $C_2H_4$ is 5.25 mol $kg^{-1}$. Although the productivity is lower than UTSA-200 and SIFSIX-2-Cu-i, it is considerably higher than SIFSIX-3-Zn, SIFSIX-1-Cu, UTSA-100a, SIFSIX-3-Ni, FeMOF-74, NOTT-300 (Table S5). The corresponding amount of $C_2H_2$ captured by Cu-PSB amounts to 98 mmol $kg^{-1}$. The comparisons of Cu-PSB with other benchmark materials are presented in Table S5. Such a high value is almost similar to that of SIFSIX-2-Cu-i, and considerably upper side of SIFSIX-3-Zn, SIFSIX-1-Cu, UTSA-100a, SIFSIX-3-Ni, FeMOF-74, NOTT-300. A similar observation was also found for the biogas and flue gas mixtures, whereby $CH_4$ and $N_2$ were eluted first, followed by $CO_2$ after some time.

It is remarkable that Cu-PSB takes up 2489.1 mmol $kg^{-1}$ (2538.9 mmol/L) of $CO_2$ from the $CO_2/CH_4$ (50:50) mixture (Fig. 4c) at 295 K (at 273 K these values are 3338.8 mmol $kg^{-1}$ or 3405.6 mmol/L). The amount of $CO_2$ captured just before exiting the adsorbed packed is very important for post-combustion $CO_2$ capture as it is directly associated with the operational cost of a PSA unit. Cu-PSB takes 1100.2 mmol $kg^{-1}$ (1122.2 mmol/L) of $CO_2$ from 15/85 $CO_2/N_2$ mixture (Fig. 4d) at 295 K (at 273 K $CO_2$ captured amount is 1781.0 mmol $kg^{-1}$ or 1816.7 mmol/L), which further re-emphasized the high potential of Cu-PSB as an exceptional candidate for the $C_2H_2/C_2H_4$ separation, and $CO_2$ capture from the bio and post-combustion flue gas mixtures.

The industrial-relevant gas separations (such as $CO_2$ and $C_2H_2$) are typically carried out under more harsh conditions. For example, in the cases of $C_2H_2/C_2H_4$ gas mixture, the $C_2H_2$ raw streams, produced from the combustion of natural gas or the cracking of hydrocarbons, typically contain a small amount of water and acidic gases [12]. On the other hand in biogas and flue gas, $CO_2$ is diluted with $CH_4$, $N_2$, water vapour, and many other acidic toxic gases [31]. Despite these complexities in realistic mixtures, the separation process mostly focused on ideal mixtures. Thus to meet this gap, researchers should use well-defined *exemplar mixtures* to urgently act in this regard [72]. However, working with such mixtures is extremely challenging compared to binary gas mixture separations and needs a much more sophisticated setup. Thus before going for such *realistic* and *process stream* exploration, the chemical stability of the materials should be confirmed [72]. In general, classical MOFs are infamous for their poor chemical stability, especially in water and pH mediums and thus, a whole lot of efforts are now being made in developing water and pH-stable MOFs to make them potential in practical environments, especially for applications in water-containing media [73–76]. Although, quite a few MOFs could be found in literature where they are stable in water and under dry acid gases such as $SO_2$, the performance is drastically reduced, and/or the framework collapses in the presence of wet conditions containing ppm levels of $SO_2$ [74]. Thus, the structural stability of Cu-PSB has been explored in different chemical environments such as, in water, boiling water, and an aqueous solution of pH = 1–11 for minimum of 7 days. The PXRD measurement revealed that all the peaks are retained and matched well with pristine Cu-PSB, strongly indicating the structural retention in those media (Fig. 5a and Figure S17). The framework is even

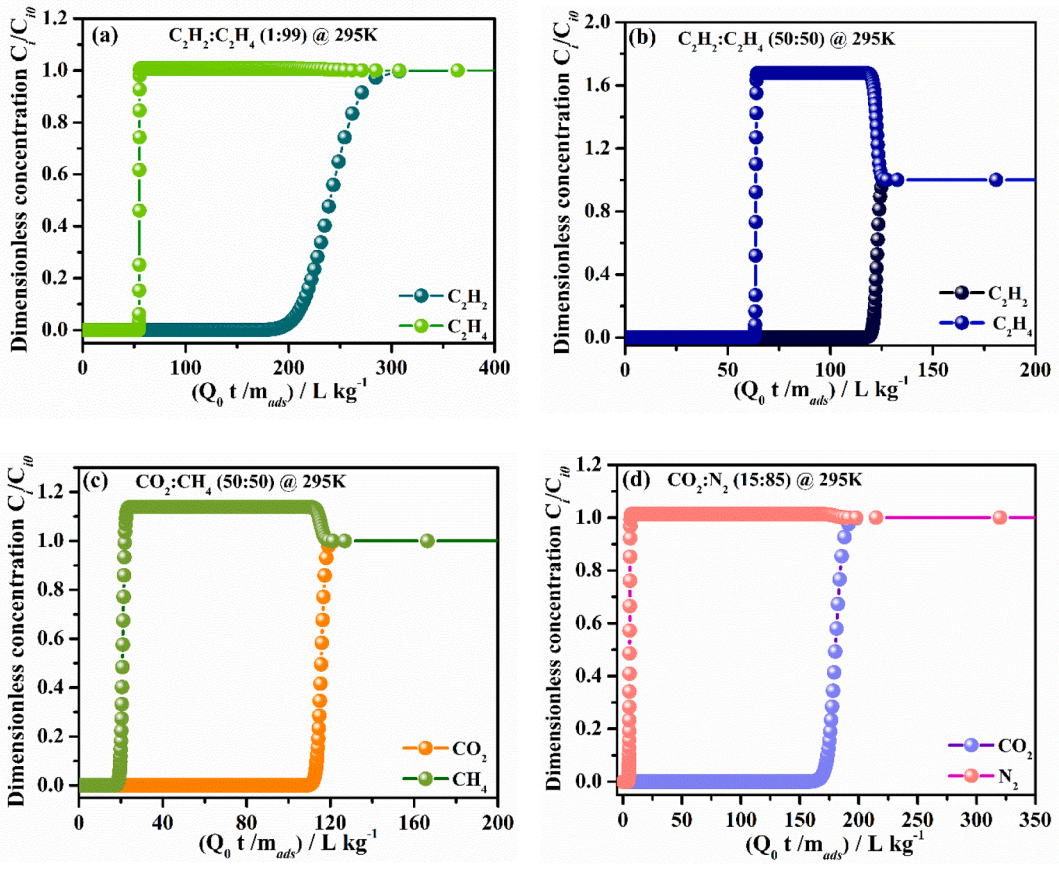


**Fig. 4.** Transient breakthrough simulations of Cu-PSB in a fixed bed operating at 100 kPa, and 295 K. (a, b) $C_2H_2/C_2H_4$ (1:99 & 50:50); (c) $CO_2/CH_4$ (50:50) and (d) $CO_2/N_2$ (15:85) mixtures. x-axis represents $\frac{Q_0 t}{m_{ads}}$ as modified time parameter.

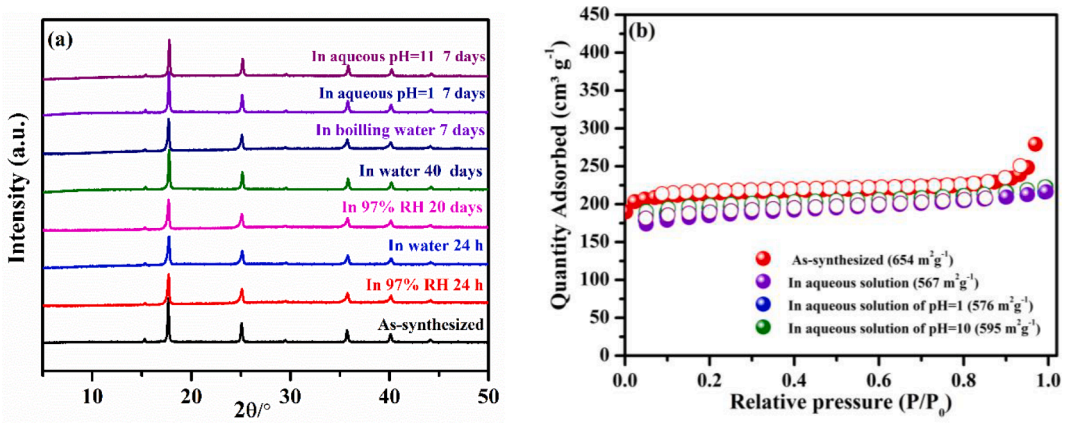


**Fig. 5.** Chemical stability of Cu-PSB. (a) PXRD pattern after exposure to different chemical environments. (b) $N_2$ adsorption after exposure to water, and an aqueous solution of pH = 1, and 10 for 24 h (BET surface area were mentioned in brackets). The filled and open circles represent the adsorption and desorption points.

stable in 6 M HCl (7 Days) and 18 M $H_2SO_4$ (Figure S17). Some MOFs show kinetic stability in some cases and subsequently transform to a thermodynamically stable phase after prolonged exposure. No such observation was found for Cu-PSB, as the PXRD pattern after 40 days of water treatment matched with the as-synthesized Cu-PSB (Fig. 5a). The high structural stability of Cu-PSB exhibited the best chemical stability among the benchmark acetylene selective MOFs such as UTSA-74, Zn-MOF-74, bio-MOF-1, TIFSIX-2-Cu-i, UTSA-300, UiO-66, ZIF-8, and NKMOF-1-Ni as shown in Table S6 [39]. Classical ZIF-8 and UiO-66 are arguably the best chemically robust MOFs and thus have been extensively investigated for numerous purposes, while Cu-PSB is even a more robust framework than ZIF-8 and UiO-66. It could be noted that ZIF-8 is stable in basic medium and unstable in acidic medium (Table S6). On the other hand, UiO-66 is stable over a wide range in pH medium (pH 1-12), however, collapses in potent acidic mediums such as in 6 M HCl and 18 M $H_2SO_4$ (Table S6). *Although the PXRD gives an indication about the structural stability, the loss of porosity and the surface area still becomes undetected.* Thus, surface area analysis after exposure to different chemical environments is an important *follow-up method* to more thoroughly determine if the MOF is stable or not [73]. The BET surface area was thus investigated from $N_2$ absorption at 77 K after treating the Cu-PSB samples in water, pH = 1, and pH = 10 for 24 h. Fig. 5b showing the $N_2$ adsorption isotherm after exposure to respective medias, the $N_2$ uptakes were 216, 216, and 222 $cm^3\ g^{-1}$, little lower to pristine Cu-PSB (279 $cm^3\ g^{-1}$). The corresponding BET surface area was calculated as 567, 576, and 595 $m^2\ g^{-1}$, respectively, which were close to the as-prepared Cu-PSB (654 $m^2\ g^{-1}$), further confirming the ultra-stable nature of the framework. Thus, Cu-PSB is an excellent candidate, having ultrahigh stability, high uptake capacity, and moderate regeneration energies for $C_2H_2$ and $CO_2$, which deserves further exploration in the presence of *realistic* and *process stream* gas mixtures.

Besides the high scalability, high gas uptake capacity, targeted selectivity, and chemical stability of a porous adsorbent, the ability to regenerate the parent material over multiple cycles is an important metrics for evaluating a porous adsorbent's economical and efficient separation potential. Thus, the cyclic adsorption performance of Cu-PSB for $CO_2$ at 273 K was also investigated (Figure S19). As observed, Cu-PSB can be easily regenerated at 295 K under in situ vacuum for 1 h without any loss in $CO_2$ capture ability minimum of up to five cycles.

## 3. Conclusion

Overall, in the search for a highly scalable and highly robust porous MOF-based adsorbent for the capture/separation with economic regeneration in a durable manner, we realized the highly efficient separation of three different gas mixtures $C_2H_2/C_2H_4$, biogas, and flue gas mixtures in a single ultra-microporous metal cyanide-based framework, namely Cu-PSB, an age-old coordination complex. Till now, such separations have been unexplored with this types of frameworks. The excellent selectivity for $C_2H_2/C_2H_4$, biogas, and flue gas separations under ambient conditions could be attributed to the dual effect of pore windows with functionalized pore channels containing open metal sites and π electron density. The ease of scale-up crystallization from the green medium at room temperature makes this MOF high potential for industrial usage. Additionally, the excellent water and chemical stability demonstrate Cu-PSB as an exceptional candidate having a high prospect of being tested for complex mixtures such as *realistic* and *process streams*.

## Funding

S.C.P. thanks IIT KGP for the SRF fellowship. M.C.D. gratefully acknowledges the financial support received from SERB, New Delhi as Core Research Grant (CRG/2019/001034).

## Declaration of Competing Interest

The authors declare that they have no known competing financial interests or personal relationships that could have appeared to influence the work reported in this paper.

## Data availability

Data available in SI

## Appendix A. Supplementary data

Instrument details, synthesis of Cu-PSB, Basic characterization data, including PXRD, TGA, EDX. Isotherm fitting, Isosteric heat of adsorption and IAST calculations, fitting plots, and Transient breakthrough details.

Supplementary data to this article can be found online at https://doi.org/10.1016/j.cej.2023.141795.

## References

[1] M. Tagliabue, D. Farrusseng, S. Valencia, S. Aguado, U. Ravon, C. Rizzo, A. Corma, C. Mirodatos, Natural gas treating by selective adsorption: Material science and chemical engineering interplay, Chem. Eng. J. 155 (2009) 553–556, https://doi.org/10.1016/j.cej.2009.09.010.

[2] S.M. Kuznicki, V.A. Bell, S. Nair, H.W. Hillhouse, R.M. Jacubinas, C.M. Braunbarth, B.H. Toby, M. Tsapatsis, A titanosilicate molecular sieve with adjustable pores for size-selective adsorption of molecules, Nature 412 (2001) 720–724, https://doi.org/10.1038/35089052.

[3] M.M. Lozinska, E. Mangano, J.P.S. Mowat, A.M. Shepherd, R.F. Howe, S. P. Thompson, J.E. Parker, S. Brandani, P.A. Wright, Understanding carbon dioxide adsorption on univalent cation forms of the flexible zeolite Rho at conditions relevant to carbon capture from flue gases, J. Am. Chem. Soc. 134 (2012) 17628–17642, https://doi.org/10.1021/ja3070864.

[4] D.S. Sholl, R.P. Lively, Seven chemical separations to change the world, Nature 532 (2016) 435–438, https://doi.org/10.1038/532435a.

[5] M.C. Das, S.C. Pal, B. Chen, Emerging microporous HOF materials to address global energy challenges, Joule 6 (2022) 22–27, https://doi.org/10.1016/j.joule.2021.12.005.

[6] R.-B. Lin, S. Xiang, W. Zhou, B. Chen, Microporous metal-organic framework materials for gas separation, Chem 6 (2020) 337–363, https://doi.org/10.1016/j.chempr.2019.10.012.

[7] H. Wang, Y. Liu, J. Li, Designer metal-organic frameworks for size-exclusion-based hydrocarbon separations: progress and challenges, Adv. Mater. 32 (2020) 2002603, https://doi.org/10.1002/adma.202002603.

[8] J.-R. Li, R.J. Kuppler, H.-C. Zhou, Selective gas adsorption and separation in metal-organic frameworks, Chem. Soc. Rev. 38 (2009) 1477–1504, https://doi.org/10.1039/B802426J.

[9] L. Li, R.-B. Lin, X. Wang, W. Zhou, L. Jia, J. Li, B. Chen, Kinetic separation of propylene over propane in a microporous metal-organic framework, Chem. Eng. J. 354 (2018) 977–982, https://doi.org/10.1016/j.cej.2018.08.108.

[10] Z. Bao, G. Chang, H. Xing, R. Krishna, Q. Rena, B. Chen, Potential of microporous metal–organic frameworks for separation of hydrocarbon mixtures, Energy Environ. Sci. 9 (2016) 3612–3641, https://doi.org/10.1039/C6EE01886F.

[11] K. Adil, Y. Belmabkhout, R.S. Pillai, A. Cadiau, P.M. Bhatt, A.H. Assen, G. Maurin, M. Eddaoudi, Gas/vapour separation using ultra-microporous metal–organic frameworks: insights into the structure/separation relationship, Chem. Soc. Rev. 46 (2017) 3402–3430, https://doi.org/10.1039/C7CS00153C.

[12] R. Sahoo, M.C. Das, $C_{2s}/C_1$ Hydrocarbon Separation: The major step towards natural gas purification by metal-organic frameworks (MOFs), Coord. Chem. Rev. 442 (2021), 213998, https://doi.org/10.1016/j.ccr.2021.213998.

[13] A.A. Lysova, K.A. Kovalenko, A.S. Nizovtsev, D.N. Dybtsev, V.P. Fedin, Efficient separation of methane, ethane and propane on mesoporous metal-organic frameworks, Chem. Eng. J. 453 (2023), 139642, https://doi.org/10.1016/j.cej.2022.139642.

[14] R. Sahoo, S. Chand, M. Mondal, A. Pal, S.C. Pal, M.K. Rana, M.C. Das, A "Thermodynamically Stable" 2D Nickel Metal-Organic Framework over a Wide pH Range with Scalable Preparation for Efficient $C_{2s}$ over $C_1$ Hydrocarbon Separations, Chem. -Eur. J. 26 (2020) 12624–12631, https://doi.org/10.1002/chem.202001611.

[15] S. Dutta, S. Mukherjee, O. T. Qazvini, A. K. Gupta, S. Sharma, D. Mahato, R. Babarao, S.ujit K. Ghosh, Three-in-One $C_2H_2$-Selectivity-Guided Adsorptive Separation across an Isoreticular Family of Cationic Square-Lattice MOFs, Angew. Chem. Int. Ed. 61 (2022) e202114132, 10.1002/anie.202114132.

[16] R. Goswami, N. Seal, S.R. Das, A. Tyagi, S. Neogi, Devising Chemically Robust and Cationic Ni(II)-MOF with Nitrogen-Rich Micropores for Moisture Tolerant $CO_2$ Capture: Highly Regenerative and Ultra-Fast Colorimetric Sensor for TNP and Multiple Oxo-Anions in Water with Theoretical Revelation, ACS Appl. Mater. Interfaces 11 (2019) 40134–40150, https://doi.org/10.1021/acsami.9b15179.

[17] A. Pal, S. Chand, M.C. Das, A Water Stable Two-Fold Interpenetrating Microporous MOF for Selective $CO_2$ Adsorption and Separation, Inorg. Chem. 56 (2017) 13991–13997, https://doi.org/10.1021/acs.inorgchem.7b02136.

[18] A. Pal, S. Chand, D. Madden, D. Franz, L. Ritter, A. Johnson, B. Space, T. Curtin, M. C. Das, A Microporous Co-MOF for Highly Selective $CO_2$ Sorption in High Loadings Involving Aryl C-H...O=C=O Interactions: Combined Simulation and Breakthrough Studies, Inorg. Chem. 58 (2019) 11553–11560, https://doi.org/10.1021/acs.inorgchem.9b01402.

[19] W. Fan, S. Yuan, W. Wang, L. Feng, X. Liu, X. Zhang, X. Wang, Z. Kang, F. Dai, D. Yuan, D. Sun, H.-C. Zhou, Optimizing Multivariate Metal-Organic Frameworks for Efficient $C_2H_2/CO_2$ Separation, J. Am. Chem. Soc. 142 (2020) 8728–8737, https://doi.org/10.1021/jacs.0c00805.

[20] Y. Wang, M. Fu, S. Zhou, H. Liu, X. Wang, W. Fan, Z. Liu, Z. Wang, D. Li, H. Hao, X. Lu, S. Hu, D. Sun, Guest-molecule-induced self-adaptive pore engineering facilitates purification of ethylene from ternary mixture, Chem 8 (2022) 3263–3274, https://doi.org/10.1016/j.chempr.2022.08.014.

[21] W. Fan, Y. Ying, S.B. Peh, H. Yuan, Z. Yang, Y.D. Yuan, D. Shi, X. Yu, C. Kang, D. Zhao, Multivariate Polycrystalline Metal−Organic Framework Membranes for $CO_2/CH_4$ Separation, J. Am. Chem. Soc. 143 (2021) 17716–17723, https://doi.org/10.1021/jacs.1c08404.

[22] Y. He, R. Krishna, B. Chen, Metal–organic frameworks with potential for energy-efficient adsorptive separation of light hydrocarbons, Energy Environ. Sci. 5 (2012) 9107–9120, https://doi.org/10.1039/C2EE22858K.

[23] E.D. Bloch, W.L. Queen, R. Krishna, J.M. Zadrozny, C.M. Brown, J.R. Long, Hydrocarbon separations in a metal-organic framework with open iron(II) coordination sites, Science 335 (2012) 1606–1610, https://doi.org/10.1126/science.1217544.

[24] X. Cui, K. Chen, H. Xing, Q. Yang, R. Krishna, Z. Bao, H. Wu, W. Zhou, X. Dong, Y. Han, B. Li, Q. Ren, M.J. Zaworotko, B. Chen, Pore chemistry and size control in hybrid porous materials for acetylene capture from ethylene, Science 353 (2016) 141–144, https://doi.org/10.1126/science.aaf2458.

[25] B. Li, X. Cui, D. O'Nolan, H.-M. Wen, M. Jiang, R. Krishna, H. Wu, R.-B. Lin, Y.-S. Chen, D. Yuan, H. Xing, W. Zhou, Q. Ren, G. Qian, M.J. Zaworotko, B. Chen, An ideal molecular sieve for acetylene removal from ethylene with record selectivity and productivity, Adv. Mater. 29 (2017) 1704210, https://doi.org/10.1002/adma.201704210.

[26] D. O'Nolan, D.G. Madden, A. Kumar, K.-J. Chen, T. Pham, K.A. Forrest, E. P. Kazmierczak, Q.-Y. Yang, C.A. Murray, C.C. Tang, B. Space, M.J. Zaworotko, Impact of partial interpenetration in a hybrid ultramicroporous material on $C_2H_2/C_2H_4$ separation performance, Chem. Commun. 54 (2018) 3488–3491, https://doi.org/10.1039/C8CC01627E.

[27] M. Jiang, X. Cui, L. Yang, Q. Yang, Z. Zhang, Y. Yang, H. Xing, A thermostable anion-pillared metal-organic framework for $C_2H_2/C_2H_4$ and $C_2H_2/CO_2$ separations, Chem. Eng. J. 352 (2018) 803–810, https://doi.org/10.1016/j.cej.2018.07.104.

[28] D. Lv, J. Chen, K. Yang, H. Wu, Y. Chen, C. Duan, Y. Wu, J. Xiao, H. Xi, Z. Li, Q. Xia, Ultrahigh $CO_2/CH_4$ and $CO_2/N_2$ adsorption selectivities on a cost-effectively L-aspartic acid based metal-organic framework, Chem. Eng. J. 375 (2019), 122074, https://doi.org/10.1016/j.cej.2019.122074.

[29] W. Fan, S.B. Peh, Z. Zhang, H. Yuan, Z. Yang, Y. Wang, K. Chai, D. Sun, D. Zhao, Tetrazole-functionalized zirconium metal-organic cages for efficient $C_2H_2/C_2H_4$ and $C_2H_2/CO_2$ separations, Angew. Chem. Int. Ed. 60 (2021) 17338–17343, https://doi.org/10.1002/anie.202102585.

[30] Y. Ye, S. Xian, H. Cui, K. Tan, L. Gong, B. Liang, T. Pham, H. Pandey, R. Krishna, P. C. Lan, K.A. Forrest, B. Space, T. Thonhauser, J. Li, S. Ma, metal−organic framework based hydrogen-bonding nanotrap for efficient acetylene storage and separation, J. Am. Chem. Soc. 144 (2022) 1681–1689, https://doi.org/10.1021/jacs.1c10620.

[31] R. Sahoo, S. Mondal, D. Mukherjee, M.C. Das, MOFs for $CO_2$ separation from flue and biogas mixtures, Adv. Funct. Mat. 32 (2022) 2207197, https://doi.org/10.1002/adfm.202207197.

[32] J.-B. Lin, T.T.T. Nguyen, R. Vaidhyanathan, J. Burner, J.M. Taylor, H. Durekova, F. Akhtar, R.K. Mah, O.G. Nik, S. Marx, N. Fylstra, S.S. Iremonger, K.W. Dawson, P. Sarkar, P. Hovington, A. Rajendran, T.K. Woo, G.K.H. Shimizu, A scalable metal-organic framework as a durable physisorbent for carbon dioxide capture, Science 374 (2022) 6574, https://doi.org/10.1126/science.abi7281.

[33] Y. Xie, R.-B. Lin, B. Chen, Old materials for new functions: recent progress on metal cyanide based porous materials, Adv. Sci. 9 (2022) 2104234, https://doi.org/10.1002/advs.202104234.

[34] S.S. Kaye, J.R. Long, Hydrogen Storage in the Dehydrated Prussian Blue Analogues $M_3[Co(CN)_6]_2$, J. Am. Chem. Soc. 127 (2005) 6506–6507, https://doi.org/10.1021/ja051168t.

[35] K.W. Chapman, P.D. Southon, C.L. Weeks, C.J. Kepert, Reversible hydrogen gas uptake in nanoporous prussian blue analogues, Chem. Commun. (2005) 3322–3324, https://doi.org/10.1039/B502850G.

[36] L. Deng, Z. Yang, L. Tan, L. Zeng, Y. Zhu, L. Guo, Investigation of the prussian blue analog $Co_3[Co(CN)_6]_2$ as an anode material for nonaqueous potassium-ion batteries, Adv. Mater. 30 (2018) 1802510, https://doi.org/10.1002/adma.201802510.

[37] J. Gao, J. Cong, Y. Wu, L. Sun, J. Yao, B. Chen, Bimetallic hofmann-type metal−organic framework nanoparticles for efficient electrocatalysis of oxygen evolution reaction, ACS Appl. Energy Mater. 1 (2018) 5140–5144, https://doi.org/10.1021/acsaem.8b01229.

[38] D. Aguila, Y. Prado, E.S. Koumousi, C. Mathonie, R. Clerac, Switchable Fe/Co Prussian blue networks and molecular analogues, Chem. Soc. Rev. 45 (2016) 203–224, https://doi.org/10.1039/C5CS00321K.

[39] J. Pei, K. Shao, J.-X. Wang, H.-M. Wen, Y. Yang, Y. Cui, R. Krishna, B. Li, G. Qian, A chemically stable Hofmann-Type metal−organic framework with sandwich-like binding sites for benchmark acetylene capture, Adv. Mater. 32 (2020) 1908275, https://doi.org/10.1002/adma.201908275.

[40] J. Gao, X. Qian, R.-B. Lin, R. Krishna, H. Wu, W. Zhou, B. Chen, Mixed metal–organic framework with multiple binding sites for efficient $C_2H_2/CO_2$ separation, Angew. Chem. Int. Ed. 59 (2020) 4396–4400, https://doi.org/10.1002/anie.202000323.

[41] Y. Liu, J. Liu, H. Xiong, J. Chen, S. Chen, Z. Zeng, S. Deng, J. Wang, Negative electrostatic potentials in a Hofmann-type metal-organic framework for efficient acetylene separation, Nat. Commun. 13 (2022) 5515, https://doi.org/10.1038/s41467-022-33271-3.

[42] D. Sensharma, D.J. O'Hearn, A. Koochaki, A.A. Bezrukov, N. Kumar, B.H. Wilson, M. Vandichel, M.J. Zaworotko, The First sulfate pillared hybrid ultramicroporous material, SOFOUR-1-Zn, and Its Acetylene Capture Properties, Angew. Chem. Int. Ed. 61 (2022) e2021161.

[43] L. Wang, W. Sun, Y. Zhang, N. Xu, R. Krishna, J. Hu, Y. Jiang, Y. He, H. Xing, Interpenetration symmetry control within ultramicroporous robust boron cluster hybrid MOFs for benchmark purification of acetylene from carbon dioxide, Angew. Chem. Int. Ed. 60 (2021) 22865–22870, https://doi.org/10.1002/anie.202107963.

[44] W. Gong, H. Cui, Y. Xie, Y. Li, X. Tang, Y. Liu, Y. Cui, B. Chen, Efficient $C_2H_2/CO_2$ Separation in Ultramicroporous Metal−Organic Frameworks with Record $C_2H_2$ storage density, J. Am. Chem. Soc. 143 (2021) 14869–14876, https://doi.org/10.1021/jacs.1c07191.

[45] Y. Zhang, J. Hu, R. Krishna, L. Wang, L. Yang, X. Cui, S. Duttwyler, H. Xing, Rational design of microporous MOFs with anionic boron cluster functionality and cooperative dihydrogen binding sites for highly selective capture of acetylene, Angew. Chem. Int. Ed. 59 (2020) 17664–17669, https://doi.org/10.1002/ange.202007681.

[46] J. Lee, C.Y. Chuah, J. Kim, Y. Kim, N. Ko, Y. Seo, K. Kim, T.H. Bae, E. Lee, separation of acetylene from carbon dioxide and ethylene by a water-stable microporous metal–organic framework with aligned imidazolium groups inside the channels, Angew. Chem. Int. Ed. 57 (2018) 7869–7873, https://doi.org/10.1002/ange.201804442.

[47] S. Yang, A.J. Ramirez-Cuesta, R. Newby, V. Garcia-Sakai, P. Manuel, S.K. Callear, S. I. Campbell, C.C. Tang, M. Schröder, Supramolecular binding and separation of hydrocarbons within a functionalized porous metal–organic framework, Nat. Chem. 7 (2015) 121–129, https://doi.org/10.1038/nchem.2114.

[48] F. Zheng, L. Guo, B. Gao, L. Li, Z. Zhang, Q. Yang, Y. Yang, B. Su, Q. Ren, Z. Bao, Engineering the pore size of pillared-layer coordination polymers enables highly efficient adsorption separation of acetylene from ethylene, ACS Appl. Mater. Interfaces 11 (2019) 28197–28204, https://doi.org/10.1021/acsami.9b09231.

[49] T.-L. Hu, H. Wang, B. Li, R. Krishna, H. Wu, W. Zhou, Y. Zhao, Y. Han, X. Wang, W. Zhu, Z. Yao, S. Xiang, B. Chen, Microporous metal–organic framework with dual functionalities for highly efficient removal of acetylene from ethylene/acetylene mixtures, Nat. Commun. 6 (2015) 7328, https://doi.org/10.1038/ncomms8328.

[50] M. Jiang, B. Li, X. Cui, Q. Yang, Z. Bao, Y. Yang, H. Wu, W. Zhou, B. Chen, H. Xing, Controlling pore shape and size of interpenetrated anion-pillared ultramicroporous materials enables molecular sieving of $CO_2$ combined with ultrahigh uptake capacity, ACS Appl. Mater. Interfaces 10 (2018) 16628–16635, https://doi.org/10.1021/acsami.8b03358.

[51] K.-J. Chen, D.G. Madden, T. Pham, K.A. Forrest, A. Kumar, Q.-Y. Yang, W. Xue, B. Space, J.J. Perry IV, J.-P. Zhang, X.-M. Chen, M.J. Zaworotko, Tuning pore size in square-lattice coordination networks for size-selective sieving of $CO_2$, Angew. Chem. 55 (2016) 10268–10272, https://doi.org/10.1002/anie.201603934.

[52] Y. Yan, M. Juríček, F.X. Coudert, N.A. Vermeulen, S. Grunder, A. Dailly, W. Lewis, A.J. Blake, J.F. Stoddart, M. Schröder, Non-interpenetrated metal-organic frameworks based on copper(II) paddlewheel and oligoparaxylene-isophthalate linkers: synthesis, structure, and gas adsorption, J. Am. Chem. Soc. 138 (2016) 3371–3381, https://doi.org/10.1021/jacs.5b12312.

[53] P.Q. Liao, D.D. Zhou, A.X. Zhu, L. Jiang, R.B. Lin, J.P. Zhang, X.M. Chen, strong and dynamic $CO_2$ sorption in a flexible porous framework possessing guest chelating claws, J. Am. Chem. Soc. 134 (2012) 17380–17383, https://doi.org/10.1021/ja3073512.

[54] R. Banerjee, A. Phan, B. Wang, C. Knobler, H. Furukawa, M. O'Keeffe, O.M. Yaghi, High-throughput synthesis of zeolitic imidazolate frameworks and application to $CO_2$ capture, Science 319 (2008) 939–943, https://doi.org/10.1126/science.1152516.

[55] H.X. Zhang, M. Liu, G.L. Xu, L.Y. Liu, J. Zhang, Selectivity of $CO_2$ via pore space partition in Zeolitic Boron Imidazolate Frameworks, Chem. Commun. 52 (2016) 3552–3555, https://doi.org/10.1039/C6CC00185H.

[56] Y.-L. Peng, T. Pham, P. Li, T. Wang, Y. Chen, K.-J. Chen, K.A. Forrest, B. Space, P. Cheng, M.J. Zaworotko, Z. Zhang, Robust ultramicroporous metal–organic frameworks with benchmark affinity for acetylene, Angew. Chem. Int. Ed. 57 (2018) 10971–10975, https://doi.org/10.1002/anie.201806732.

[57] O.T. Qazvini, R. Babarao, S.G. Telfer, Multipurpose metal−organic framework for the adsorption of acetylene: ethylene purification and carbon dioxide removal, Chem. Mater. 31 (2019) 4919–4926, https://doi.org/10.1021/acs.chemmater.9b01691.

[58] S.-C. Xiang, Z. Zhang, C.-G. Zhao, K. Hong, X. Zhao, D.-R. Ding, M.-H. Xie, C.-D. Wu, M.C. Das, R. Gill, K.M. Thomas, B. Chen, Rationally tuned micropores within enantiopure metal-organic frameworks for highly selective separation of acetylene and ethylene, Nat. Commun. 2 (2011) 1–7, https://doi.org/10.1038/ncomms1206.

[59] A.Ö. Yazaydın, A.I. Benin, S.A. Faheem, P. Jakubczak, J.J. Low, R.R. Willis, R. Q. Snurr, Enhanced $CO_2$ adsorption in metal-organic frameworks via occupation of open-metal sites by coordinated water molecules, Chem. Mater. 21 (2009) 1425–1430, https://doi.org/10.1021/cm900049x.

[60] Z. Xiang, X. Peng, X. Cheng, X. Li, D. Cao, CNT@$Cu_3$(BTC)$_2$ and metal–organic frameworks for separation of $CO_2$/$CH_4$ Mixture, J. Phys. Chem. C 115 (2011) 19871, https://doi.org/10.1021/jp206959k.

[61] P. Nugent, Y. Belmabkhout, S.D. Burd, A.J. Cairns, R. Luebke, K. Forrest, T. Pham, S. Ma, B. Space, L. Wojtas, M. Eddaoudi, M.J. Zaworotko, Porous materials with optimal adsorption thermodynamics and kinetics for $CO_2$ separation, Nature 495 (2013) 80–84, https://doi.org/10.1038/nature11893.

[62] B. Wang, A.P. Coté, H. Furukawa, M. O'Keeffe, O.M. Yaghi, Colossal cages in zeolitic imidazolate frameworks as selective carbon dioxide reservoirs, Nature 453 (2008) 207–211, https://doi.org/10.1038/nature06900.

[63] A. Pal, S. Chand, D. G. Madden, D. Franz, L. Ritter, B. Space, T. Curtin, S. C. Pal, M. C. Das, Immobilization of a polar sulfone moiety onto the pore surface of a humid-stable MOF for highly efficient $CO_2$ separation under dry and wet environments through direct $CO_2$–sulfone interactions, ACS Appl. Mater. Interfaces 12 (2020) 41177–41184, 10.1021/acsami.0c07380.

[64] Z.H. Rada, H.R. Abid, J. Shang, Y. He, P. Webley, S. Liu, H. Sun, S. Wang, Effects of amino functionality on uptake of $CO_2$, $CH_4$ and selectivity of $CO_2$/$CH_4$ on Titanium based MOFs, Fuel 160 (2015) 318–327, https://doi.org/10.1016/j.fuel.2015.07.088.

[65] Y. Xiong, Y.Z. Fan, R. Yang, S. Chen, M. Pan, J.J. Jiang, C.Y. Su, Amide and N-oxide functionalization of T-shaped ligands for isoreticular MOFs with giant enhancements in $CO_2$ separation, Chem. Commun. 50 (2014) 14631–14634, https://doi.org/10.1039/C4CC06697A.

[66] H. Alawisi, B. Li, Y. He, H.B. Arman, A. Asiri, H. Wang, B. Chen, A microporous metal-organic framework constructed from a new tetracarboxylic acid for selective gas separation, Cryst. Growth Des. 14 (2014) 2522–2526, https://doi.org/10.1021/cg500235j.

[67] J.R. Li, J. Yu, W. Lu, L.B. Sun, J. Sculley, P.B. Balbuena, H.C. Zhou, Porous materials with pre-designed single-molecule traps for $CO_2$ selective adsorption, Nat. Commun. 4 (2013) 1538–1545, https://doi.org/10.1038/ncomms2552.

[68] B. Wang, H. Huang, X.L. Lv, Y. Xie, M. Li, J.R. Li, Tuning $CO_2$ selective adsorption over $N_2$ and $CH_4$ in UiO-67 analogues through ligand functionalization, Inorg. Chem. 53 (2014) 9254–9259, https://doi.org/10.1021/ic5013473.

[69] R. Krishna, J.R. Long, Screening metal-organic frameworks by analysis of transient breakthrough of gas mixtures in a fixed bed adsorber, J. Phys. Chem. C 115 (2011) 12941–12950, https://doi.org/10.1021/jp202203c.

[70] S. Xiang, Y. He, Z. Zhang, H. Wu, W. Zhou, R. Krishna, B. Chen, Microporous Metal-organic Framework with Potential for Carbon Dioxide Capture at Ambient Conditions, Nat. Commun. 3 (2012) 954–963, https://doi.org/10.1021/acsami.0c07380.

[71] S. Chand, A. Pal, M.C. Das, A. Moisture-Stable, 3D Microporous CoII-Metal–Organic Framework with Potential for Highly Selective $CO_2$ Separation under Ambient Conditions, Chem.—Eur. J. 24 (2018) 5982–5986, https://doi.org/10.1002/chem.201800693.

[72] D.S. Sholl, R.P. Lively, Exemplar mixtures for studying complex mixture effects in practical chemical separations, JACS Au 2 (2022) 322–327, https://doi.org/10.1021/jacsau.1c00490.

[73] N.C. Burtch, H. Jasuja, K.S. Walton, Water Stability and Adsorption in Metal−Organic Frameworks, Chem. Rev. 114 (2014) 10575–10612, https://doi.org/10.1021/cr5002589.

[74] S. Han, Y. Huang, T. Watanabe, Y. Dai, K.S. Walton, S. Nair, D.S. Sholl, J. C. Meredith, High-Throughput Screening of Metal−Organic Frameworks for $CO_2$ Separation, ACS Comb. Sci. 14 (2012) 263–267, https://doi.org/10.1021/co3000192.

[75] S.C. Pal, R. Ahmed, A.K. Manna, M.C. Das, Potential of a pH-Stable Microporous MOF for $C_2H_2$/$C_2H_4$ and $C_2H_2$/$CO_2$ Gas Separations under Ambient Conditions, Inorg. Chem. 61 (2022) 18293–18302, https://doi.org/10.1021/acs.inorgchem.2c03275.

[76] X.-P. Fu, Y.-L. Wang, X.-F. Zhang, R. Krishna, C.-T. He, Q.-Y. Liu, B. Chen, Collaborative pore partition and pore surface fluorination within a metal–organic framework for high-performance $C_2H_2$/$CO_2$ separation, Chem. Eng. J. 432 (2022), 134433, https://doi.org/10.1016/j.cej.2021.134433.

# Supporting Information (SI)

## Highly Scalable Acid-Base Resistant Cu-Prussian Blue Metal–Organic Framework for $C_2H_2/C_2H_4$, BioGas, and Flue Gas Separations

Shyam Chand Pal[a] Rajamani Krishna[b]* and Madhab C. Das[a]*

[a]*Department of Chemistry, Indian Institute of Technology Kharagpur, Kharagpur 721302, WB, India. E-mail: mcdas@chem.iitkgp.ac.in*

[b]*Van 't Hoff Institute for Molecular Sciences, University of Amsterdam, Science Park 904, 1098 XH Amsterdam, The Netherlands E-mail: r.krishna@contact.uva.nl*

## Table of Contents

## 1. Synthetic Procedure

### I. Materials.

All starting chemicals and solvents were commercially available and could be directly used without further purification. $Cu(NO_3)_2 \cdot 3H_2O$ was purchased from Merck, and Potassium hexacyanocobaltate (III) was purchased from Sigma-Aldrich.

### II. Synthesis of $K_aCu_b[Co(CN)_6]_2[H_2O]_6 \cdot xH_2O$, (Cu-PSB)

Cu-PSB was synthesized by following the already reported procedure.[1,2] $K_3[Co(CN)_6]$ (664 mg, 2 mmol) in 15 mL water was added dropwise to an aqueous solution of $Cu(NO_3) \cdot 3H_2O$ (1047 mg, 3.6 mmol) and stirred at room temperature overnight. The resulting precipitate was obtained as a sea blue microcrystalline powder, which was isolated by filtration after 24 h from the mother liquor and washed with a copious amount of water. The product was then dried in the desiccator. The formula was determined with the help of EDX and TGA analysis. From EDX, the ratio of the metals (K: Co: Cu) was found to be 0.04, 3.95, and 5.32. TGA showed a weight loss of 19.57% at 155 °C. The composition of Cu-PSB is**,** therefore, $K_{0.02}Cu_{2.7}[Co(CN)_6]_2[H_2O]_6 \cdot 2H_2O$, which is consistent with the elemental analysis. It is to be noted that the degree of hydration varies upon the variations in humidity and sample storage conditions.

## 2. Physical Measurements.

The FT-IR spectra were recorded in the 400-4000 $cm^{-1}$ on a Perkin-Elmer RX1 spectrophotometer. PXRD patterns were recorded using *Cu-*$K_\alpha$ radiation (1.5418 Å) on a Bruker D8 Advance diffractometer. Thermogravimetric analysis (TGA) was performed using a TG 209 *F3* Tarsus (Netzsch), and the sample was heated from room temperature to 800 °C at a rate of 5 °C $min^{-1}$ under an $N_2$ atmosphere. Gas sorption experiments were tested on a Micromeritics *3-Flex* Surface Characterization Analyzer at different temperatures. All the guest water molecules in the framework were removed by degassing the sample at 373 K for 24 h until the outgassing rate was five μmHg/min prior to measurements. The sorption measurement was maintained at 77K K by using a liquefied $N_2$, and a chiller was used for adsorption isotherms at 273 and 295 K, respectively.

## 3. Fitting of pure component isotherms

The unary isotherms for $C_2H_2$, $C_2H_4$, $C_2H_6$, and $CO_2$ measured at two different temperatures 273 K, and 295 K in Cu-PSB were fitted with excellent accuracy using either the dual-site Langmuir model, where we distinguish two distinct adsorption sites A and B:

$$q = \frac{q_{sat,A} b_A p}{1 + b_A p} + \frac{q_{sat,B} b_B p}{1 + b_B p} \tag{S1}$$

In eq (S1), the Langmuir parameters $b_A, b_B$ are both temperature dependent

$$b_A = b_{A0} \exp\left(\frac{E_A}{RT}\right); \quad b_b = b_{B0} \exp\left(\frac{E_B}{RT}\right) \tag{S2}$$

In eq (S2), $E_A, E_B$ are the energy parameters associated with sites A, and B, respectively.

The unary isotherms for $CH_4$, and $N_2$ measured at two different temperatures 273 K, and 295 K in Cu-PSB were fitted with excellent accuracy using the single-site Langmuir model.

The unary isotherm fit parameters are provided in **Error! Reference source not found.**.

## 4. Isosteric heat of adsorption

The isosteric heat of adsorption, $Q_{st}$, is defined as

$$Q_{st} = -RT^2 \left(\frac{\partial \ln p}{\partial T}\right)_q \tag{S3}$$

where, the derivative in the right member of eq (S3) is determined at constant adsorbate loading, $q$. the derivative was determined by analytic differentiation of the combination of eq (S1), eq (S2), and eq (S3).

## 5. IAST calculations of adsorption selectivities

For separation of binary mixtures of components 1 and 2, the adsorption selectivity, $S_{ads}$, is defined by

$$S_{ads} = \frac{q_1 / q_2}{y_{10} / y_{20}} \tag{S4}$$

In eq (S4), $y_{10}, y_{20}$ are the mole fractions of the bulk gas phase mixture.

The molar loadings $q_1, q_2$ of the two components are determined using the Ideal Adsorbed Solution Theory (IAST) of Myers and Prausnitz[3] using the unary isotherm fits as data inputs. IAST calculations were carried out for $C_2H_2/C_2H_4$ (1:99 & 50:50); $CO_2/CH_4$ (50:50) and $CO_2/N_2$ (15:85) mixtures at 273 K and 295 K.

## 6. Transient breakthrough simulations

Transient breakthrough simulations for $C_2H_2/C_2H_4$ (1:99 & 50:50); $CO_2/CH_4$ (50:50) and $CO_2/N_2$ (15:85) mixtures were carried out for the adsorption cycle in a fixed bed operating at a total pressure of 100 kPa, and temperatures of 273 K and 295 K. The simulation methodology is described in earlier publications.[4-8] In these simulations, intra-crystalline diffusion influences are ignored. For these simulations we specify: length of packed bed, $L$ = 0.3 m; cross-sectional area, $A$ = 1 m$^2$; volumetric flow rate at the entrance to the bed, $Q_0 = 40$ L s$^{-1}$; voidage of the packed bed, $\varepsilon$ = 0.4. The volume of MOF used in the simulations is $V_{ads} = LA(1-\varepsilon)$. It is important to note that the volume of adsorbent, $V_{ads}$, includes the pore volume of the adsorbent material. If $\rho$ is the framework density, the mass of the adsorbent in the bed is $m_{ads} = (1-\varepsilon)\times(L \text{ m})\times(A \text{ m}^2)\times(\rho \text{ kg m}^{-3})$ kg.

It is to be noted that the dimensions of the breakthrough tube used in the simulations is different from those used in previous works.[9,10] The $C_2H_4$ productivity values and $C_2H_2$ capture capacities are not influenced by the dimensions of the tube, because these are expressed per kg of adsorbent in tube.

For presentation of the results of the breakthrough simulations, the dimensionless concentrations at the exit, $c_i/c_{i0}$ are plotted as a function of the parameters

$\frac{\left(Q_0 = \text{flow rate L s}^{-1}\right)\times\left(\text{time in s}\right)}{\left(\text{kg MOF packed in tube}\right)} = \frac{Q_0 t}{m_{ads}} = \text{L kg}^{-1}$. It is also to be noted that we use the modified time parameter $\frac{Q_0 t}{m_{ads}}$ instead of the dimensionless breakthrough time, $\tau$, used in earlier works of Cui *et al* and Das *et al*.[9,10]

## 7. Notation

| | |
|---|---|
| $b$ | Langmuir constant, $\text{Pa}^{-1}$ |
| $c_i$ | molar concentration of species $i$, mol $\text{m}^{-3}$ |
| $c_{i0}$ | molar concentration of species $i$ in fluid mixture at inlet, mol $\text{m}^{-3}$ |
| $q$ | component molar loading of species $i$, mol $\text{kg}^{-1}$ |
| $q_{sat}$ | saturation loading, mol $\text{kg}^{-1}$ |
| $Q_0$ | volumetric flow rate of gas mixture at inlet, L $\text{s}^{-1}$ |
| $L$ | length of packed bed adsorber, m |
| $m_{ads}$ | mass of adsorbent in packed bed, kg |
| $t$ | time, s |
| $T$ | absolute temperature, K |

***Greek letters***

| | |
|---|---|
| $\varepsilon$ | voidage of packed bed, dimensionless |
| $\rho$ | framework density, kg $\text{m}^{-3}$ |
| $\tau$ | time, dimensionless |

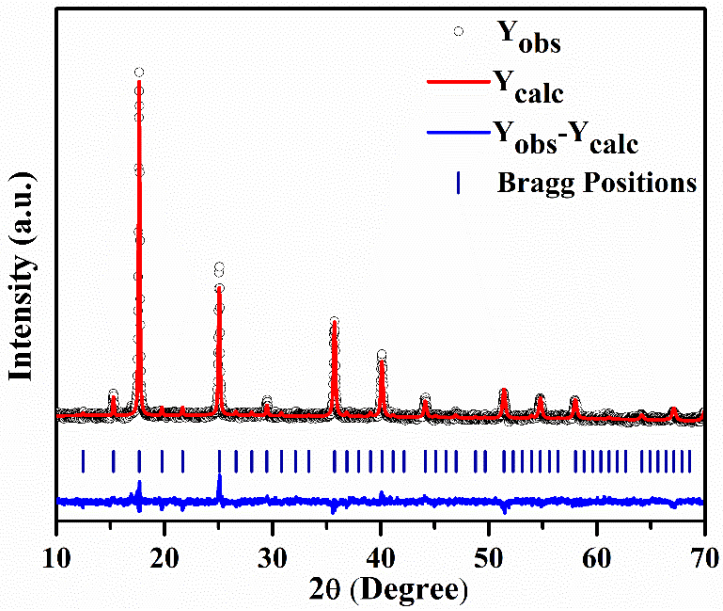


**Figure S1**: Rietveld Refinement of powder X-ray diffraction pattern of **Cu-PSB** (R(obs) = 9.65, and wR (obs)=8.77) and GOF=1.31.[2]

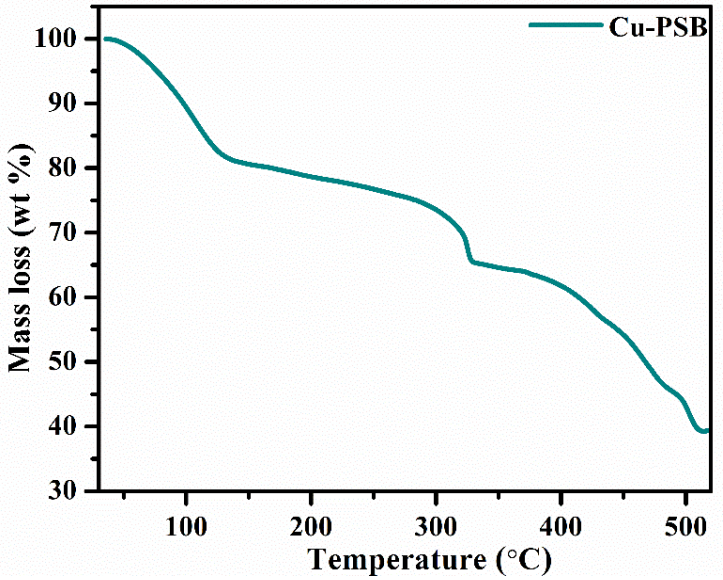


**Figure S2**: Thermogravimetric analysis (TGA) profile for **Cu-PSB**.

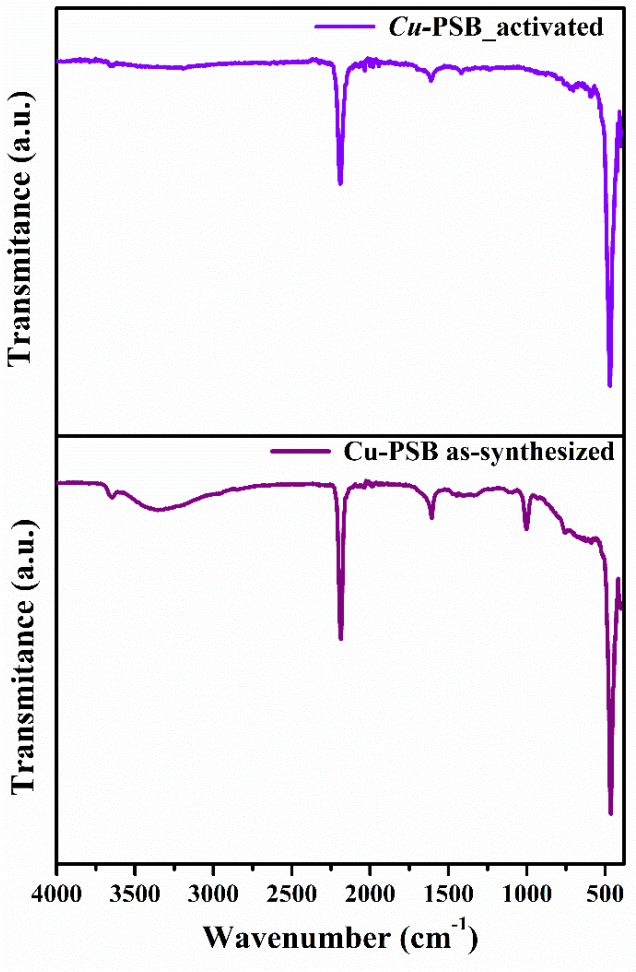


**Figure S3**: ATR-IR spectra of as-synthesized and activated sample of **Cu-PSB**.

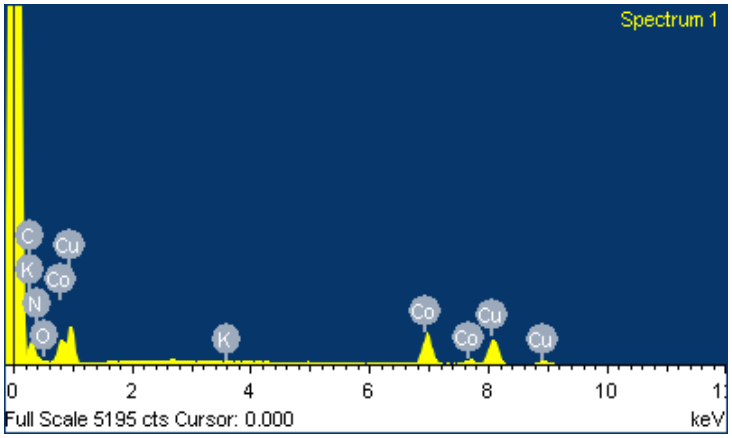


**Figure S4**: EDS spectra of **Cu-PSB**. The atomic molar ratio of Cu/Co is 1.34.

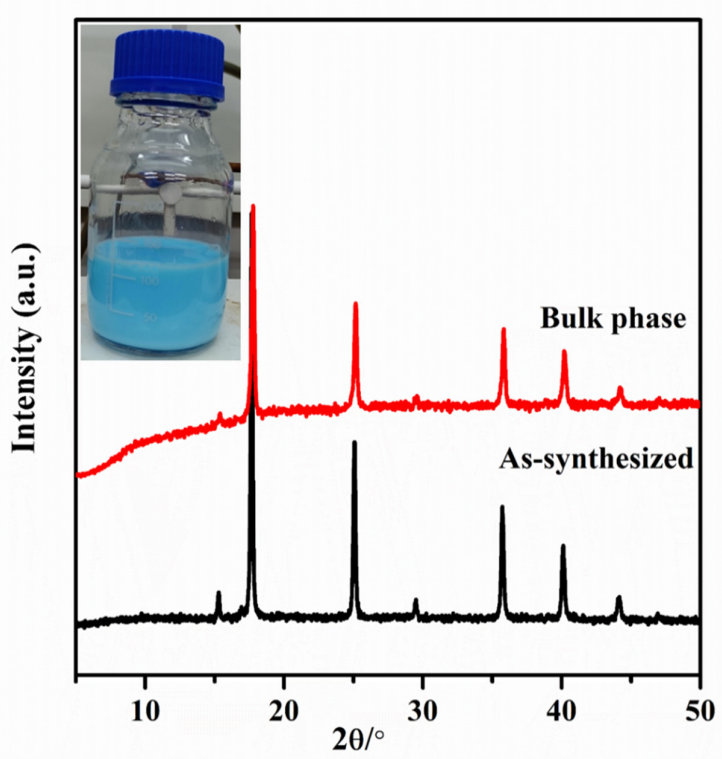


**Figure S5**: PXRD patterns of *G*-scale and as-synthesized **Cu-PSB**.

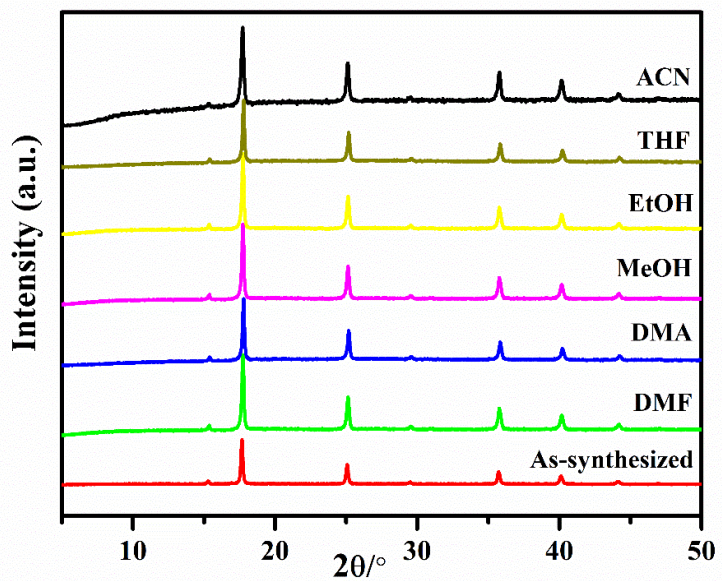


**Figure S6**: Chemical stability test of **Cu-PSB** after exposure to different common organic solvents for 7 days.

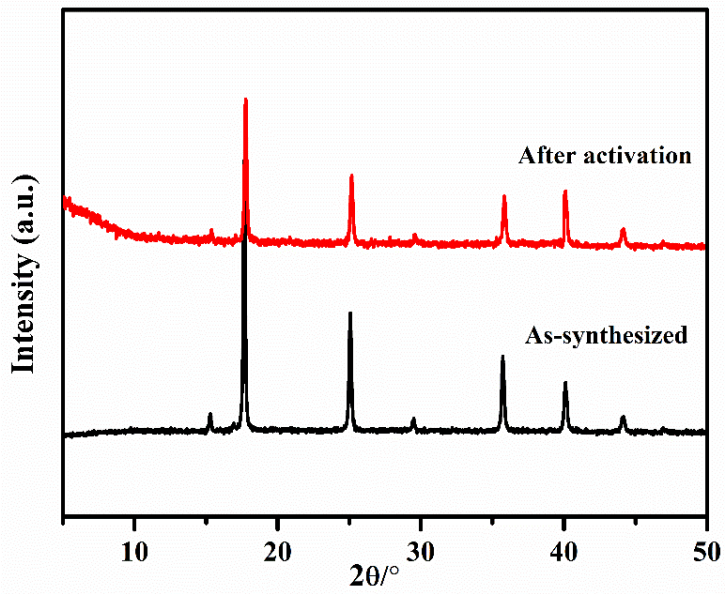


**Figure S7**: Activated and as-synthesized PXRD patterns of **Cu-PSB**.

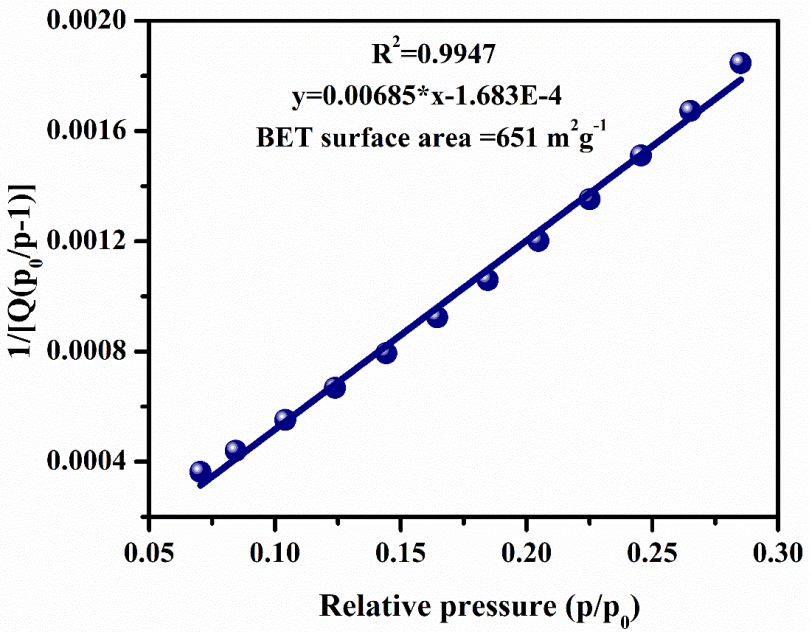


**Figure S8**: BET surface area of **Cu-PSB** determined from $N_2$ adsorption at 77K.

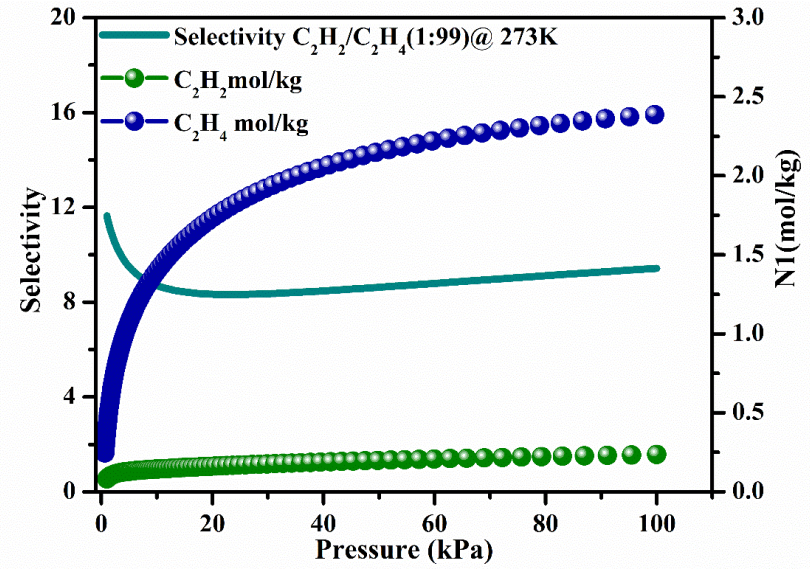


**Figure S9**: $C_2H_2/C_2H_4$ (1:99) separation selectivity and loading amounts in mixed gas phase predicated from IAST at 273 K of **Cu-PSB**.

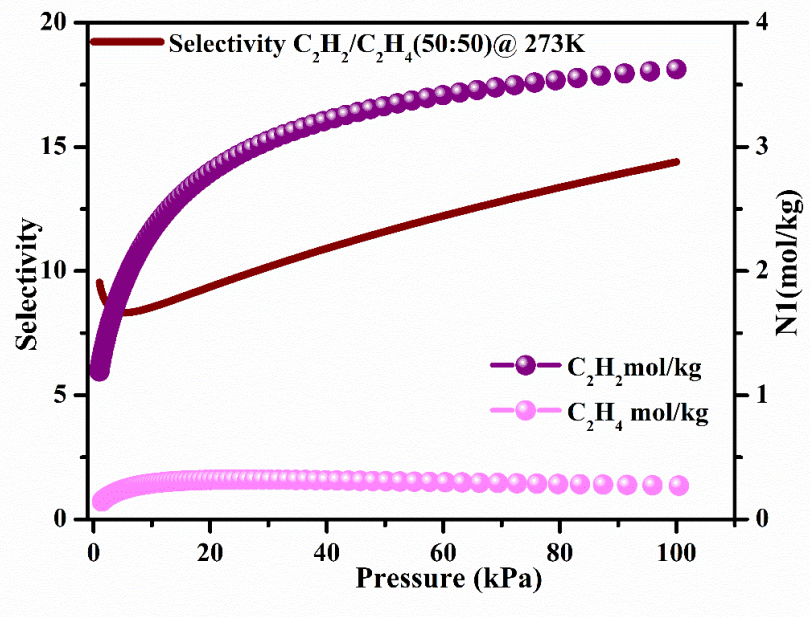


**Figure S10**: $C_2H_2/C_2H_4$ (50:50) separation selectivity and loading amounts in mixed gas phase predicated by IAST at 273 K of **Cu-PSB**.

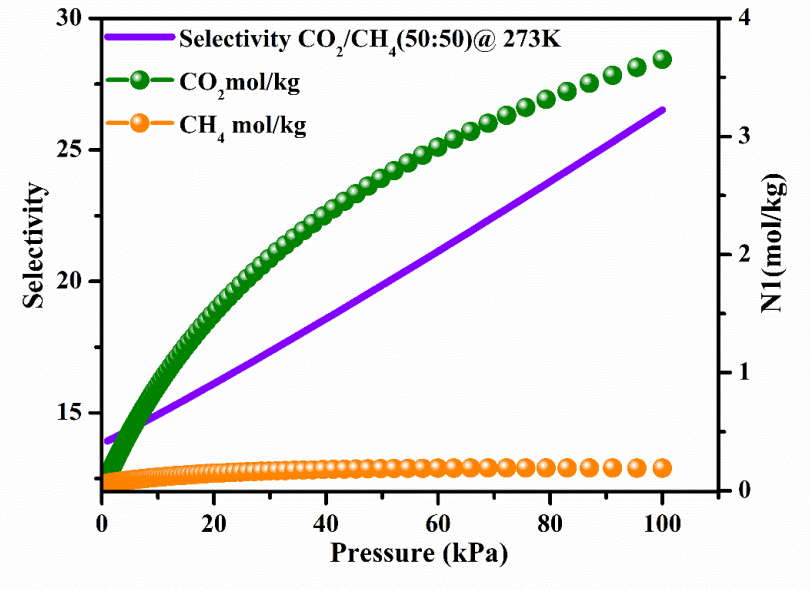


**Figure S11**: $CO_2/CH_4$ (50:50) separation selectivity and loading amounts in mixed gas phase predicated from IAST at 273 K of **Cu-PSB**.

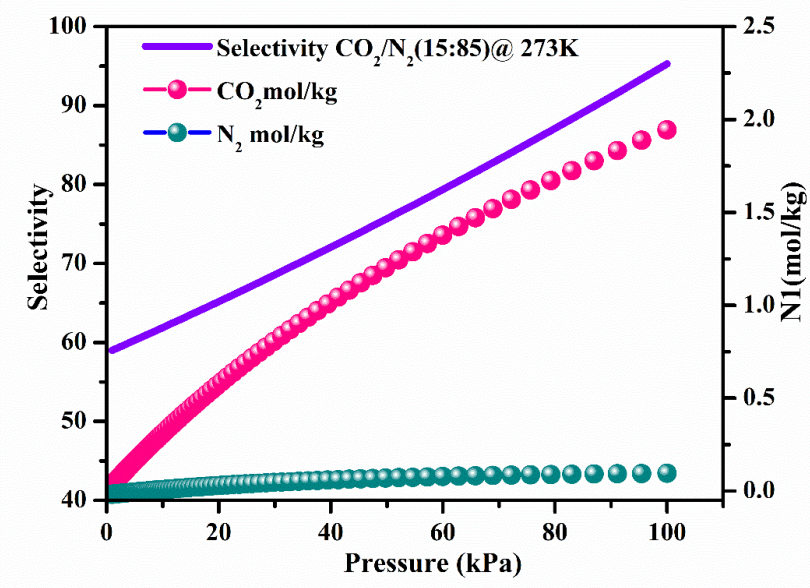


**Figure S12**: $CO_2/N_2$ (15:85) separation selectivity and loading amounts in mixed gas phase predicated from IAST at 273 K of **Cu-PSB**.

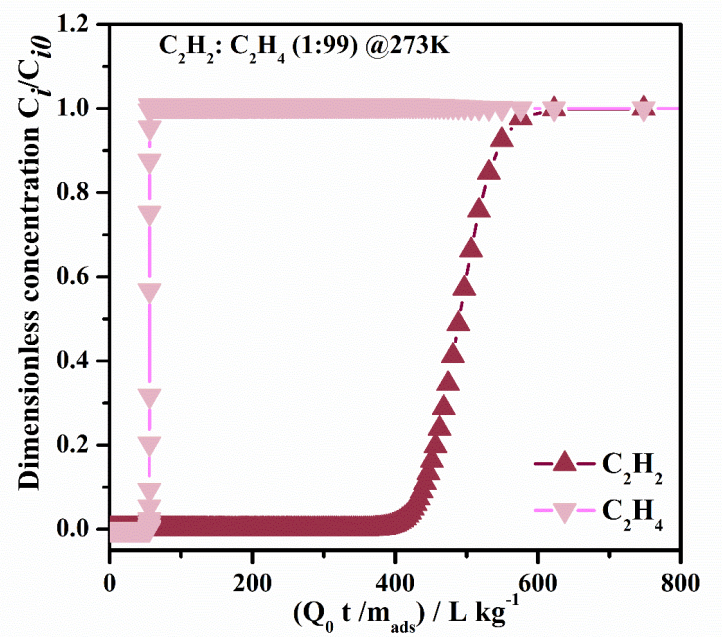


**Figure S13**: Breakthrough simulation result for **Cu-PSB** for the separation of $C_2H_2/C_2H_4$ (1:99) mixture in a fixed bed operating at a total pressure of 100 kPa, and temperature of 273 K. The x-axis represents $\frac{Q_0 t}{m_{ads}}$ as modified time parameter.

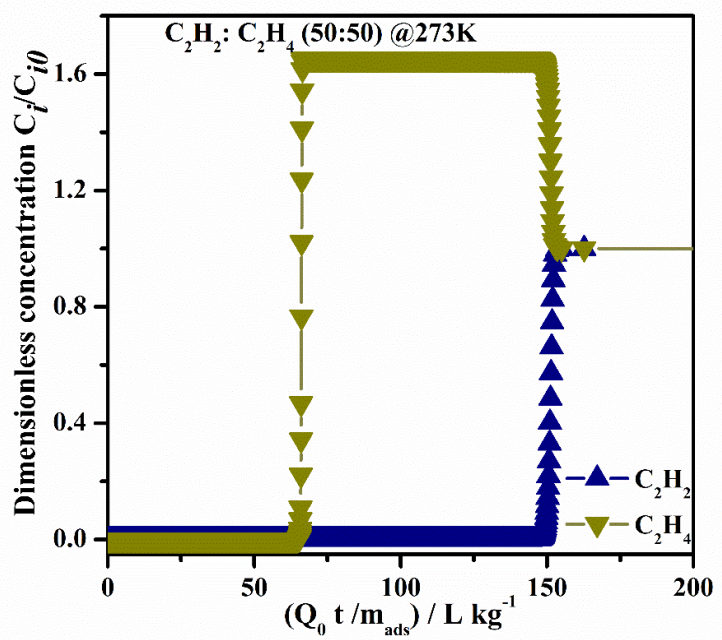


**Figure S14**: Breakthrough simulation result for **Cu-PSB** for the separation of $C_2H_2/C_2H_4$ (50:50) mixture in a fixed bed operating at a total pressure of 100 kPa, and temperature of 273 K. The x-axis represents $\frac{Q_0 t}{m_{ads}}$ as modified time parameter.

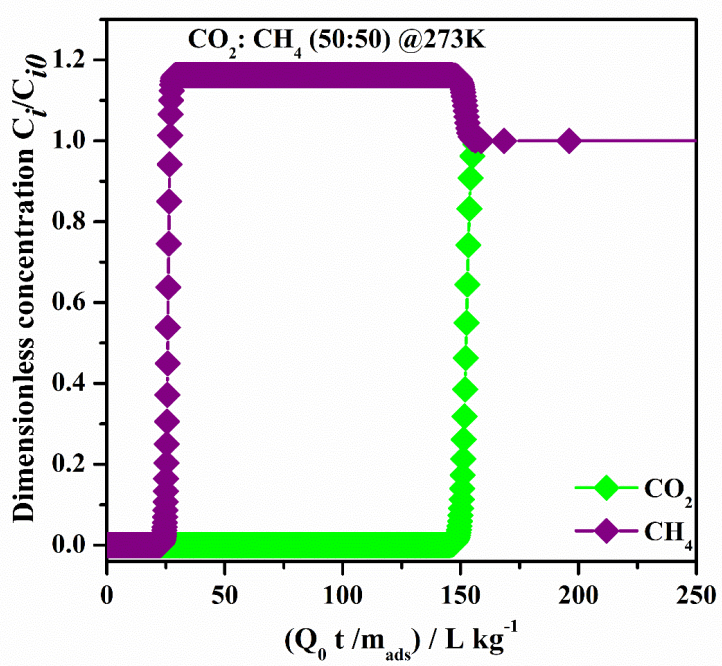


**Figure S15**: Breakthrough simulation result for **Cu-PSB** for separation of $CO_2/CH_4$ (50:50) mixture in a fixed bed operating at a total pressure of 100 kPa, and temperature of 273 K. The x-axis represents $\frac{Qt}{m_{ads}}$ as modified time parameter.

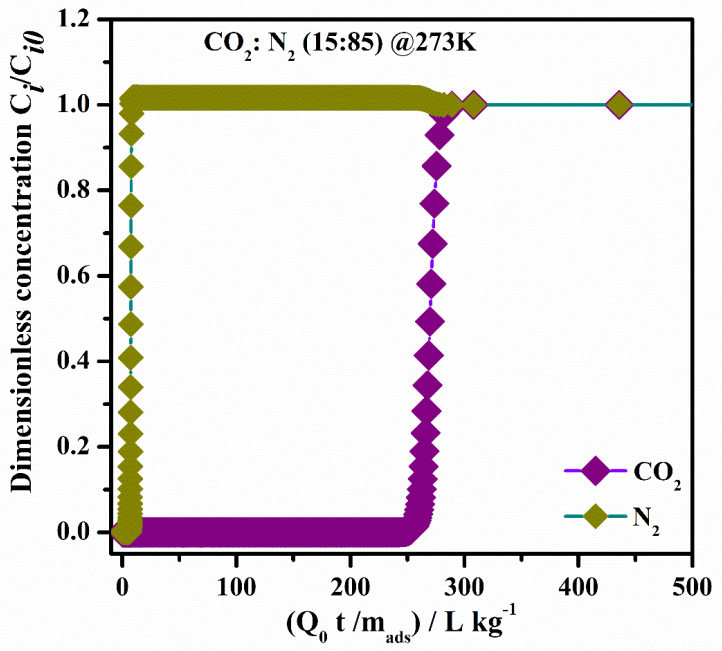


**Figure S16**: Breakthrough simulation result for **Cu-PSB** for separation of $CO_2/N_2$ (15:85) mixture in a fixed bed operating at a total pressure of 100 kPa, and temperature of 273 K. The x-axis represents $\frac{Qt}{m_{ads}}$ as modified time parameter.

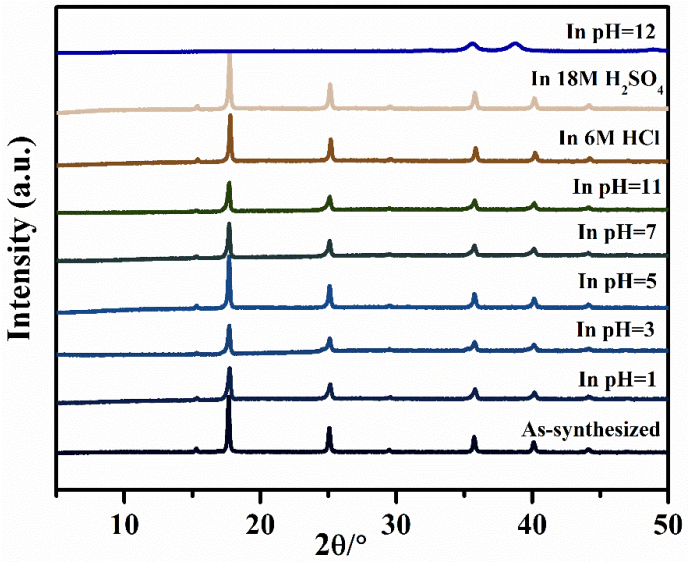


**Figure S17**: PXRD patterns of **Cu-PSB** after exposure to different pH (aqueous HCl and aqueous NaOH was used for different pH) and in 6M HCl for 7 days, 18M $H_2SO_4$ for 24 h. At pH=12 the solutions became black after one hour, indicating degradation of the framework.

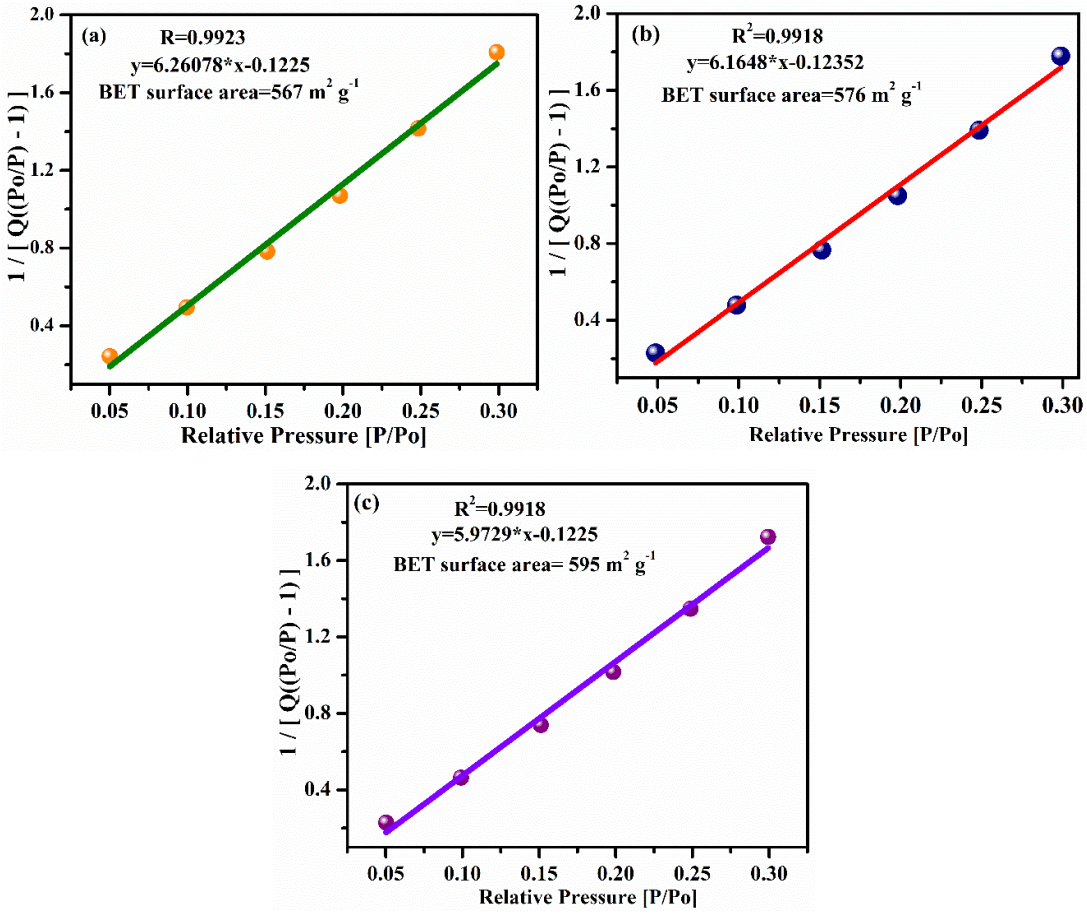


**Figure S18**: BET surface area determined from 77K $N_2$ adsorption of Cu-PSB after exposure to different chemical environments for 24 h (a) water (b) aqueous solution of pH=1, and (c) aqueous solution of pH=10.

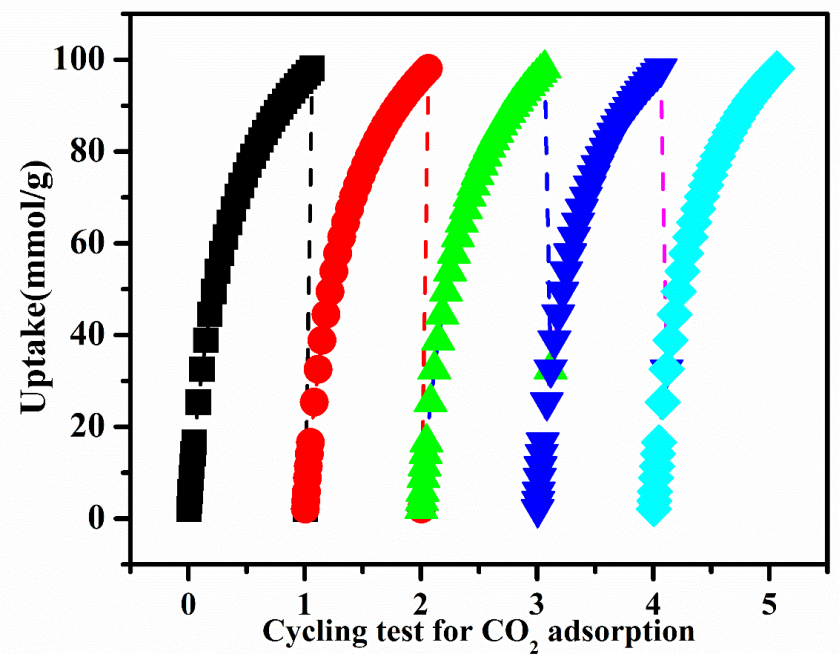


**Figure S19**: Cyclic adsorption test for $CO_2$ at 273K.

**Table S1.** Comparison of $C_2H_2$ uptake, $C_2H_2/C_2H_4$ uptake ratio and heat of adsorption data of **Cu-PSB** with some of the $C_2H_2$ selective MOFs at 298K.

| MOFs | Surface area BET ($m^2\ g^{-1}$)# | Pore (Å) | $C_2H_2$ uptake (mmol/g) at 1 bar | $C_2H_4$ uptake (mmol/g) at 1 bar | $C_2H_2/C_2H_4$ uptake ratio | $C_2H_2/C_2H_4$ IAST Selectivity (1:99) | $-Q_{st}$ of $C_2H_2$ (kJ/mol) | Ref |
|---|---|---|---|---|---|---|---|---|
| **Cu-PSB** | 651 | ~4.4×4.4[$] | 3.52[b] | 2.36[b] | 1.49 | 4.5[b] | 20-42 | **This work** |
| **Mg-MOF-74** | 927 | 11×11 | 8.37[c] | 7.45[c] | 1.12 | 2.18 | 41 | S11 |
| **NOTT–300** | 1370 | 6.5×6.5 | 6.34[d] | 4.28[d] | 1.48 | 2.3 | 32 | S12 |
| **SIFSIX-2Cu-i** | 503 | 5.2×5.2 | 4.02 | 2.19 | 1.84 | 44.54 | 41.9 | S9 |
| **SIFSIX-2-Cu** | 1881 | 10.5×10.5 | 5.38 | 2.02 | 2.66 | 6.0 | 26.3 | |
| **SIFSIX-1-Cu** | 1178 | 8.0×8.0 | 8.50 | 4.11 | 2.06 | 10.63 | 30/37[k] | |
| **SIFSIX-3-Zn** | 250 | 4.2×4.2 | 3.64 | 2.24 | 1.62 | 8.82 | 21/31[k] | |
| **SIFSIX-3-Ni** | 368 | 4.2×4.2 | 3.30 | 1.75 | 1.88 | 5.03 | 30.5 | |
| **CPL-5** | 523[a] | 11.0×6.0 | 3.01 | 1.84 | 1.64 | 5.99 | 31.3 | S13 |
| **NUC-2** | 1072 | 11.1×11.1<br>12.6×12.6 | 2.99 | 0.60 | 4.98 | 8.1 | 39.8 | S14 |
| **ZUL-100** | 548 | 3.6×4.1<br>3.1×4.4 | 5.31 | 2.76 | 1.92 | 175 | 65.3 | S15 |
| **ZUL-200** | 471 | 3.6×4.1<br>3.3×4.4 | 4.69 | 1.99 | 2.35 | 114 | 57.6 | |
| **NKMOF-1-Ni** | 380 | 5.75×5.75 | 2.72 | 2.11 | 1.28 | 51.65 | 18.8/54[f] | S16 |
| **Zu-33** | 424 | 3.0 | 3.21 | 0.59 | 6.08 | 1100 | 43.6 | S17 |
| **CPL-1** | 414[a] | 4.0×6.0 | 2.07 | 0.31 | 6.68 | 26.75 | 40.2 | S13 |
| **UTSA-100a** | 970 | 4.3×4.3 | 4.27[h] | 1.66[h] | 2.57 | 10.72[h] | 22 | S18 |
| **UTSA-200a** | 612[a] | 3.4×3.4 | 3.65 | 0.63 | 5.79 | 6320 | 40 | S19 |
| **UTSA-300a** | 311 | 3.4×3.3 | 3.08 | 0.04 | 77 | >10000[e] | 57.6 | S20 |
| **M′MOF-3a** | 110.1 | 3.4×4.8 | 1.9[h] | 0.4[h] | 4.75 | 24.03 | 27.1 | S21 |
| **ZJU-74** | 694 | 3.6 | 3.82[h] | - | - | 24.2 | 45–65 | S22 |
| **Cu(bpy)NP** | 459[a] | 6.0 × 7.0 | 2.26 | 1.82 | 1.24 | 28.5 | 40.8 | S23 |
| **$\{[Mn_3(bipy)_3(H_2O)_4]$-$[Mn(CN)_6]_2\cdot 2(bipy)\cdot 4H_2O\}_n$** | 362[g] | 5.5×4.0 | 2.65[d] | 0.24[c] | - | 16[d] | 32.4 | S24 |
| **Nbu-1** | 368.2 | 4×4 | 2.67 | 2.0 | 1.33 | 5.9 (50:50) | 38.3 | S25 |
| **Zn-atz-oba** | 710.7 | - | 2.77 | 2.03 | 1.36 | 1.43 (50:50) | 27.49 | S26 |
| **MUF-17** | 247 | - | 3.01[d] | 2.15[d] | 1.4 | 8.73 (50:50) | 49.5 | S27 |
| **MECS-5** | 964[g] | 4.5 × 5.3<br>3.4 × 4.5<br>1.8 × 3.9 | 3.85 | 1.14 | 3.37 | 12.6 | 26.09 | S28 |
| **UTSA-60a** | 484 | 4.8×4.0<br>3.6×2.8<br>3.7×10.5 | 3.12 | 2.05 | 1.52 | ~5.5 | 36 | S29 |
| **JCM-1** | 550 | 3.9 | 3.41 | 1.59 | 2.14 | 13.2 | 36.9 | S30 |
| **TIFSIX-2-Cu-i** | 685 | 9.6, 11.5^ | 4.1 | 2.5 | 1.64 | 55 | 46.3 | S31 |

[#] BET surface area from 77K $N_2$ adsorption. [a] BET surface area from 195K $CO_2$ adsorption.

[b] At temperature of 295K [c] At temperature of 273K

[d] At temperature of 293K [e]Simulated selectivity

[f] $-Q_{st}$ at various surface area coverage [g]Langmuir Surface area at 195K $CO_2$ adsorption

[h]At temperature of 296K

[$] pore window measured from the Diamond by fitting a dummy sphere of appropriate radius.

[^]Two oppositely F···F distance

**Tables S2:** Comparison of $CO_2$ loading in some well-known MOFs.

| MOF | Surface area BET ($m^2\ g^{-1}$) and Langmuir | $CO_2$ loading ($cm^3\ g^{-1}$) (273 K, 1.0 bar) | $CO_2$ loading ($cm^3\ g^{-1}$) (298 K, 1.0 bar) | Ref. |
|---|---|---|---|---|
| **Cu-PSB** | **651 (BET) 1,003 (Langmuir)** | **108** | **84** | **This work** |
| **MFM-130** | 2173 (BET) | 109 | 59 | S32 |
| **MAF-23** | 387 (BET) | 74.2 | 56.1 | S33 |
| **ZIF-69** | 1070(Langmuir) | 70 | 40.6 | S34 |
| **Zn(ain)$_2$·(DMF)** | - | 66.4 | 51.3 | S35 |
| **BIF-41** | - | 77 | 63.5 (294) | S36 |
| **HKUST-1** | 1571(BET) | 78.2 | 67.2 | S37 |
| **MIL-101Cr** | 3237(BET) | 78.6 | 53.3(293K) | S38 |
| **CPM-200s-In** | 888/1244 | 109.6 | 61.7 | S39 |
| **NENU-520** | 387(BET) | 80.4 | 60.7 | S40 |
| **UTSA-120** | 638(BET) | - | 112 (296K) | S41 |
| **SIFSIX - 2 - Cu - i** | 735 (BET) | - | 121.2 | |

**Table S3.** Dual-site Langmuir parameter fits for $C_2H_2$, $C_2H_4$, $CO_2$, $CH_4$, and $N_2$ in **Cu-PSB**.

| | Site A | | | Site B | | |
|---|---|---|---|---|---|---|
| | $\frac{q_{A,sat}}{\text{mol/kg}}$ | $\frac{b_{A0}}{\text{Pa}^{-1}}$ | $\frac{E_A}{\text{kJ mol}^{-1}}$ | $\frac{q_{B,sat}}{\text{mol/kg}}$ | $\frac{b_{B0}}{\text{Pa}^{-1}}$ | $\frac{E_B}{\text{kJ mol}^{-1}}$ |
| $C_2H_2$ | 3.1 | 1.14E-12 | 42.5 | 1.2 | 1.99E-06 | 20.0 |
| $C_2H_4$ | 1.4 | 1.06E-09 | 23.5 | 1.6 | 5.42E-05 | 6.0 |
| $CO_2$ | 5.1 | 4.80E-10 | 24.4 | 1.4 | 1.25E-07 | 14.6 |
| $CH_4$ | 2.85 | 3.13E-08 | 11.8 | | | |
| $N_2$ | 1.95 | 6.34E-09 | 13.0 | | | |

**Table S4:** Thoroughly studied developed MOFs for both flue gas (15:85 binary mixture of $CO_2/N_2$) and biogas (50:50 binary mixture of $CO_2/CH_4$) separation selectivity at 1 bar pressure.

| MOFs | Surface area BET ($m^2\ g^{-1}$) | IAST selectivity | | Temp (K) | Ref |
|---|---|---|---|---|---|
| | | $CO_2/N_2$ (15:85) | $CO_2/CH_4$ (50:50) | | |
| **Cu-PSB** | **651** | **60.5** | **14.7** | **295** | **This work** |
| **IITKGP-5** | 366 | 147.8 | 23.8 | 295 | S42 |
| **IITKGP-6** | 279 | 42.8 | 5.1 | 295 | S43 |
| **IITKGP-7** | 141 | 121.4 | 8.8 | 295 | S44 |
| **IITKGP-8** | 224 | 43.7 | 17.1 | 295 | S45 |
| **IITKGP-11** | 253 | 149.07 | 7.91 | 295 | S46 |
| **UTSA -16** | 628 | 314.7 | 29.8 | 296 | S47 |
| **UTSA -120** | 638 | ~600 | 100 | 296 | S41 |
| **SIFSIX - 2 - Cu - i** | 735 | 140 | 33 | 296 | |
| **ZJNU -44** | 2314 | ~15 | 5.5 | 296 | S48 |
| **Qc - 5 -Cu -sql - β** | 222 | 40000 | 3300 | 293 | S49 |

| | | | | | |
|---|---|---|---|---|---|
| **CSMCRI - 3** | 1814 | 128 | 11.7 | 273 | S50 |
| **CSMCRI - 9** | 469 | 43 | 5.39 | 273 | S51 |
| **MAF -66** | 1014 | 185[#] | 5.8[#] | 298 | S52 |
| **MFM -137** | 1749 | 15.7 | 4.08 | 298 | S53 |
| **MFM -136** | 1634 | 23.2 | 3.35 | 298 | |
| **NJU -Bai52** | 1908 | 581 | 13.5 | 298 | S54 |
| **PCN -222** | 1371 | 32.8 | 4.3 | 298 | S55 |
| **IISERP - MOF26** | 210.6 | 145 | 15 | 298 | S56 |
| **HKUST - 1** | 1317 | 29.1 | 10 | 273 | S57 |
| **MIP-202** | 278.6 | 72.9 | $1.95 \times 10^6$ | 298 | S58 |
| **NKU -521** | 1100 | 56 | 22 | 298 | S59 |
| **MFM-126** | 1004 | 39.6 | 11.7 | 298 | S60 |
| **MUF-16** | 214 | 631 | - | 293 | S61 |
| **IISERP-MOF2** | 470 | 1853 | - | 313 | S62 |
| **UTSA-90** | 2273 | 21.7 | 5.3 | 295 | S63 |
| **UTSA-93** | 523 | 28 | 7.4 | 298 | S64 |
| **ZJNU-26** | 1182 | 37.3 | 4.3 | 298 | S65 |
| **ZJNU-44** | 2314 | 15 | 5.5 | 296 | S48 |
| **Qc-5-Ni-dia** | 664 | 36 | 7 | 293 | S49 |
| **Qc-5-Cu-dia** | 488 | 19 | 3 | 293 | |
| **Ni-4PyC** | 1076 | 51 | 6 | 298 | S66 |
| **NJU-Bai33** | 884.8 | 40.3 | 8.9 | 298 | S67 |
| **NJU-Bai50** | 2015 | 30.5 | 4.4 | 298 | S68 |
| **PCN-88** | 3308 | 15.2 | 7 | 296 | S69 |
| **MOF-505** | 1104 | 27.8 | 7.6 | 298 | S70 |
| [#]Henry's Law selectivity | | | | | |

**Table S5.** Comparison of the dimensionless breakthrough time for separation of $C_2H_2/C_2H_4$ mixture (1/99). The product gas stream contains less than 40 ppm $C_2H_2$.

| **MOFs** | **$C_2H_4$ productivity mol $kg^{-1}$** | **$C_2H_2$ captured mmol $kg^{-1}$** | **Temp (K)** | **Ref** |
|---|---|---|---|---|
| **Cu-PSB** | **5.25** | **98.04** | **295** | **This work** |
| **UTSA-200** | 25.52 | 258.04 | 298 | S19 |
| **SIFSIX-2-Cu-i** | 10.07 | 104.25 | 298 | |
| **SIFSIX-1-Cu** | 4.44 | 51.18 | 298 | |
| **SIFSIX-3-Zn** | 1.88 | 22.34 | 298 | |
| **UTSA-100a** | 1.72 | 19.68 | 298 | |
| **SIFSIX-3-Ni** | 0.94 | 12.91 | 298 | |
| **FeMOF-74** | 0.53 | 14.90 | 318 | |
| **M'MOF-3a** | 1.06 | 11.35 | 298 | |
| **NOTT-300** | 0.41 | 10.72 | 293 | |

**Table S6.** Comparison of the chemical stability of **Cu-PSB** with some C2H2 selective stable porous materials after treatment under various chemical environments.[S22]

| MOFs | Water | Boiling water | pH=1 | pH=12 | 6M HCl | 18M $H_2SO_4$ | Ref |
|---|---|---|---|---|---|---|---|
| Cu-PSB | √ | √ | √ | b | √ | √ | This work |
| ZJU-74 | √ | √ | √ | √ | √ | √ | S22 |
| UiO-66 | √ | √ | √ | √ | × | × | S71 |
| bio-MOF-1 | √ | √ | × | √ | × | × | S72 |
| ZIF-8 | √ | √ | × | √ | × | × | S73 |
| UTSA-74 | × | × | × | × | × | × | S74 |
| Zn-MOF-74 | √ | × | × | √ | × | × | S75 |
| TIFSIX-2-Cu-i | × | × | × | × | × | × | S76 |
| SIFSIX-3-Ni | × | × | × | × | × | × | |
| UTSA-300 | × | × | × | × | × | × | S20 |
| HOF-3 | × | × | × | × | × | × | S77 |
| NKMOF-1-Ni | √ | a | √ | √ | a | a | S16 |
| JCM-1 | √ | × | × | × | × | × | S30 |
| FJU-90 | √ | × | × | × | × | × | S78 |
| JNU-1 | √ | a | × | √ | a | a | S79 |
| HOF-21 | √ | a | a | a | a | a | S80 |
| ZUL-100 | √ | a | √ | √ | | | S14 |
| ZUL-200 | √ | a | √ | √ | a | a | |
| | | | | | | | |

[a] The stability in the corresponding conditions was not reported in the literatures.

[b]Stable upto pH=11

**References:**


1. Steven S. Kaye, J. R. Long, Hydrogen Storage in the Dehydrated Prussian Blue Analogues $M_3[Co(CN)_6]_2$, J. Am. Chem. Soc. 127 (2005) 6506-6507, https://doi.org/10.1021/ja051168t.
2. J. J. Gallegos, J. R. Herna´ndez, H. Y.-Madeira, E. Reguera, Structure of porous copper prussian blue analogues: Nature of their high $H_2$ storage capacity, J. Phys. Chem. C 114, (2010), 5043–5048, https://doi.org/10.1021/jp910544j.
3. A. L. Myers, J. M. Prausnitz, Thermodynamics of mixed gas adsorption. *A.I.Ch.E.J.* **1965**, *11*, 121-130.
4. R. Krishna, The Maxwell-Stefan description of mixture diffusion in nanoporous crystalline materials. Microporous Mesoporous Mater. 185 (2014) 30-50, https://doi.org/10.1016/j.micromeso.2013.10.026.
5. R. Krishna, Methodologies for evaluation of metal-organic frameworks in separation applications, *RSC Adv. 5* (2015) 52269-52295, https://doi.org/10.1039/C5RA07830J.
6. R. Krishna, Screening metal-organic frameworks for mixture separations in fixed-bed adsorbers using a combined selectivity/capacity metric, *RSC Adv.* 7 (2017) 35724-35737, https://doi.org/10.1039/C7RA07363A.
7. R. Krishna, Methodologies for screening and selection of crystalline microporous materials in mixture Separations, *Sep. Purif. Technol.* 194 (2018) 281-300. https://doi.org/10.1016/j.seppur.2017.11.056.

8. R. Krishna, Metrics for evaluation and screening of metal-organic frameworks for applications in mixture separations, *ACS Omega* **2020**, *5*, 16987−17004. https://doi.org/10.1021/acsomega.0c02218.
9. X. Cui, K. Chen, H. Xing, Q. Yang, R. Krishna, Z. Bao, H. Wu, W. Zhou, X. Dong, Y. Han, B. Li, Q. Ren, M.J. Zaworotko, B. Chen, Pore Chemistry and Size Control in Hybrid Porous Materials for Acetylene Capture from Ethylene, Science 353 (2016) 141-144, https://doi.org/10.1126/science.aaf2458.
10. M. C. Das, Q. Guo, Y. He, J. Kim, C. G. Zhao, K. Hong, S. Xiang, Z. Zhang, K.M. Thomas, R. Krishna, B. Chen, Interplay of Metalloligand and Organic Ligand to Tune Micropores within Isostructural Mixed-Metal Organic Frameworks (M'MOFs) for Their Highly Selective Separation of Chiral and Achiral Small Molecules, J. Am. Chem. Soc. 134 (2012) 8703-8710.
11. Y. He, R. Krishna, B. Chen, Metal–organic frameworks with potential for energy-efficient adsorptive separation of light hydrocarbons, Energy Environ. Sci. 5 (2012) 9107, https://doi.org/10.1039/C2EE22858K.
12. S. Yang, A. J. Ramirez-Cuesta, R. Newby, V. Garcia-Sakai, P. Manuel, S. K. Callear, S. I. Campbell, C. C. Tang, M. Schröder, Supramolecular binding and separation of hydrocarbons within a functionalized porous metal–organic framework. Nat. Chem. 7 (2015) 121–129, https://doi.org/10.1038/nchem.2114.
13. F. Zheng, L. Guo, B. Gao, L. Li, Z. Zhang, Q. Yang, Y. Yang, B. Su, Q. Ren, Z. Bao, Engineering the pore size of pillared-layer coordination polymers enables highly efficient adsorption separation of acetylene from ethylene, ACS Appl. Mater. Interfaces 11 (2019) 28197−28204, https://doi.org/10.1021/acsami.9b09231.
14. H. Chen, G. -L. Zhuang, F. Liming, X. Zhang, L.-N. Gaod, D. Sun, A highly robust heterometallic $Tb^{III}/Ni^{II}$–organic framework for $C_2$ hydrocarbon separation and capture, Chem. Commun. 56 (2020) 2047, https://doi.org/10.1039/C9CC09425C.
15. J. Shen, X. He, T. Ke, R. Krishna, J. M. van Baten, R. Chen, Z. Bao, H. Xing, M. Dincă, Z. Zhang, Q. Yang, Q. Ren, Simultaneous interlayer and interlayer space control in two-dimensional metal−organic frameworks for acetylene/ethylene separation, Nat Commun 11 (2020) 6259 https://doi.org/10.1038/s41467-020-20101-7.
16. Y. -L. Peng, T. Pham, P. Li, T. Wang, Y. Chen, K. -J. Chen, K. A. Forrest, B. Space, P. Cheng, M. J. Zaworotko, Z. Zhang, Robust ultramicroporous metal–organic frameworks with benchmark affinity for acetylene, Angew. Chem. Int. Ed. 57 (2018) 10971 –10975, https://doi.org/10.1002/anie.201806732.
17. Z. Zhang, X. Cui, L. Yang, J. Cui, Z. Bao, Q. Yang, H. Xing, Hexafluorogermanate (GeFSIX) anion-functionalized hybrid ultramicroporous materials for efficiently trapping acetylene from ethylene, Ind. Eng. Chem. Res. 2018, 57, 7266−7274, https://doi.org/10.1021/acs.iecr.8b00950.
18. T.-L. Hu, H. Wang, B. Li, R. Krishna, H. Wu, W. Zhou, Y. Zhao, Y. Han, X. Wang, W. Zhu, Z. Yao, S. Xiang, B. Chen, Microporous metal–organic framework with dual functionalities for highly efficient removal of acetylene from ethylene/acetylene mixtures, Nat. Commun. *6* (2015) 7328, https://doi.org/10.1038/ncomms8328.
19. B. Li, X. Cui, D. O'Nolan, H.-M. Wen, M. Jiang, R. Krishna, H. Wu, R.-B. Lin, Y.-S. Chen, D. Yuan, H. Xing, W. Zhou, Q. Ren, G. Qian, M. J. Zaworotko, B. Chen, An ideal molecular sieve for acetylene removal from ethylene with record selectivity and productivity, Adv. Mater. 29 (**2017**) 1704210, https://doi.org/10.1002/adma.201704210.
20. R. -B. Lin, L. Li, H. Wu, H. Arman, B. Li, R.-G. Lin, W. Zhou, B. Chen, Optimized separation of acetylene from carbon dioxide and ethylene in a microporous material. J. Am. Chem. Soc. 139, (2017) 8022−8028, https://doi.org/10.1021/jacs.7b03850.

21. S. -C. Xiang, Z. Zhang, C. -G. Zhao, K. Hong, X. Zhao, D.-R. Ding, M.-H. Xie, C.-D. Wu, M. C. Das, R. Gill, K. M. Thomas, B. Chen, Rationally tuned micropores within enantiopure metal-organic frameworks for highly selective separation of acetylene and ethylene, *Nat. Commun.* 2, (2011) 1−7, https://doi.org/10.1038/ncomms1206.
22. J. Pei, K. Shao, J.-X. Wang, H.-M. Wen, Y. Yang, Y. Cui, R. Krishna, B. Li, G. Qian, A chemically stable hofmann-type metal−organic framework with sandwich-like binding sites for benchmark acetylene capture, *Adv. Mater.* 32, (2020) 1908275, https://doi.org/10.1002/adma.201908275.
23. Y. Liu, J. Liu, H. Xiong, J. Chen, S. Chen, Z. Zeng, S. Deng, J. Wang, Negative electrostatic potentials in a Hofmann-type metal-organic framework for efficient acetylene separation, *Nat. Commun.* 13 (2022) 5515, https://doi.org/10.1038/s41467-022-33271-3.
24. A. Hazra, S. Jana, S. Bonakala, S. Balasubramanian, T. K. Maji, Separation/purification of ethylene from an acetylene/ethylene mixture in a pillared-layer porous metal–organic framework, Chem. Commun, 53 (2017) 4907, https://doi.org/10.1039/C7CC00726D.
25. J. Li, L. Jiang, S. Chen, A. Kirchon, B. Li, Y. Li, H. -C. Zhou, Metal–organic framework containing planar metal-binding sites: efficiently and cost-effectively enhancing the kinetic separation of $C_2H_2/C_2H_4$, J. Am. Chem. Soc. 141, (2019) 3807, https://doi.org/10.1021/jacs.8b13463.
26. J.-W. Cao, S. Mukherjee, T. Pham, Y. Wang, T. Wang, T. Zhang, X. Jiang, H.-J. Tang, K. A. Forrest, B. Space, M. J. Zaworotko, K.-J. Chen, One-step ethylene production from a four-component gas mixture by a single physisorbent. Nat. Commun. 12, (2021) 6507, https://doi.org/10.1038/s41467-021-26473-8.
27. O. T. Qazvini, R. Babarao, S. G. Telfer, Multipurpose Metal−organic framework for the adsorption of acetylene: ethylene purification and carbon dioxide removal, Chem. Mater. 31, (2019) 4919−4926, https://doi.org/10.1021/acs.chemmater.9b01691.
28. X.-J. Hong, Q. Wei, Y.-P. Cai, B.-b. Wu, H.-X. Feng, Y. Yu, R.-F. Dong, Pillar-layered metal−organic framework with sieving effect and pore space partition for effective separation of mixed gas $C_2H_2/C_2H_4$, ACS *Appl. Mater. Interfaces* 9, (**2017**) 29374−29379, https://doi.org/10.1021/acsami.7b10420.
29. H. -M. Wen, B. Li, H. Wang, C. Wu, K. Alfooty, R. Krishna, B. Chen, A microporous metal–organic framework with rare lvt topology for highly selective $C_2H_2/C_2H_4$ separation at room temperature, Chem. Commun. *51* (2015) 5610-5613, https://doi.org/10.1039/C4CC09999K.
30. J. Lee, C. Y. Chuah, J. Kim, Y. Kim, N. Ko, Y. Seo, K. Kim, T. H. Bae, E. Lee, Separation of acetylene from carbon dioxide and ethylene by a water-stable microporous metal–organic framework with aligned Imidazolium groups inside the Channels, *Angew. Chem. Int. Ed.* **2018**, *57*, 7869 –7873, https://doi.org/10.1002/anie.201804442.
31. A. Bajpai, D. O'Nolan, D. G. Madden, K. J. Chen, T. Pham, A. Kumar, M. Lusi, J. J. Perry, B. Space, M. J. Zaworotko, The effect of centred versus offset interpenetration on $C_2H_2$ sorption in hybrid ultramicroporous materials. Chem. Commun. 53 (2017) 11592, https://doi.org/10.1039/C7CC05882A.
32. Y. Yan, M. Juríček, F. X. Coudert, N. A. Vermeulen, S. Grunder, A. Dailly, W. Lewis, A. J. Blake, J. F. Stoddart, M. Schröder, Non-Interpenetrated metal-organic frameworks based on copper(II) paddlewheel and oligoparaxylene-Isophthalate linkers: synthesis, structure, and gas Adsorption *J. Am. Chem. Soc.* 138, (2016) 3371-3381, https://doi.org/10.1021/jacs.5b12312.

33. P. Q. Liao, D. D. Zhou, A. X. Zhu, L. Jiang, R. B. Lin, J. P. Zhang, X. M. Chen, Strong and dynamic $CO_2$ sorption in a flexible porous framework possessing guest chelating claws, J. Am. Chem. Soc. 134 (**2012**) 17380-17383, https://doi.org/10.1021/ja3073512.
34. R. Banerjee, A. Phan, B. Wang, C. Knobler, H. Furukawa, M. O'Keeffe, O. M. Yaghi, High-Throughput Synthesis of zeolitic imidazolate frameworks and application to $CO_2$ capture. Science 319 (2008) 939-943, https://doi.org/10.1126/science.1152516.
35. F. Wang, Y. X. Tan, H. Yang, Y. Kang, J. Zhang, Open diamondoid amino-functionalized MOFs for $CO_2$ Capture, *Chem. Commun.* 48 (**2012**) 4842-4844, https://doi.org/10.1039/C2CC31211E.
36. H. X. Zhang, M. Liu, G. L. Xu, L. Y. Liu, J. Zhang, Selectivity of $CO_2$ via pore space partition in zeolitic boron imidazolate frameworks. Chem. Commun. 52 (2016) 3552-3555, https://doi.org/10.1039/C6CC00185H.
37. Z. Liang, M. Marshall, A. L. Chaffee, $CO_2$ adsorption-based separation by metal organic framework (Cu-BTC) versus Zeolite (13X), Energy Fuels. 23 (2009) 2785-2789, https://doi.org/10.1021/ef800938e.
38. A. Khutia, C. Janiak, Programming MIL-101Cr for selective and enhanced $CO_2$ adsorption at low pressure by postsynthetic amine functionalization. *Dalton Trans. 43* (2014) 1338-1347, https://doi.org/10.1039/C3DT52365A.
39. Q. G. Zhai, X. H. Bu, C. Y. Mao, X. Zhao, P. Y. Feng, Systematic and dramatic tuning on gas sorption performance in heterometallic metal−organic frameworks, J. Am. Chem. Soc. 138 (2016) 2524-2527, https://doi.org/10.1021/jacs.5b13491.
40. S. -J. Bao, R. Krishna, Y.-B. He, J.-S. Qin, Z.-M. Su, S.-L. Li, W. Xie, D.-Y. Du, W.-W. He, S.-R. Zhang, Y.-Q. Lan, A stable metal–organic framework with suitable pore sizes and rich uncoordinated nitrogen atoms on the internal surface of micropores for highly efficient $CO_2$ capture. J. Mater. Chem. A. *3* (**2015**) 7361-7367, https://doi.org/10.1039/C5TA00256G.
41. H.-M. Wen, C. Liao, L. Li, A. Alsalme, Z. Alothman, R. Krishna, H. Wu, W. Zhou, J. Hu, B. Chen, A metal–organic framework with suitable pore size and dual functionalities for highly efficient postcombustion $CO_2$ capture. J. Mater. Chem. A, 2019, 7, 3128, https://doi.org/10.1039/C8TA11596F.
42. A. Pal, S. Chand, S. M. Elahi, M. C. Das, A microporous MOF with a polar pore surface exhibiting excellent selective adsorption of $CO_2$ from $CO_2$–$N_2$ and $CO_2$–$CH_4$ gas mixtures with high $CO_2$ loading. Dalton Trans. 46 (2017) 15280-15286, https://doi.org/10.1039/C7DT03341A.
43. A. Pal, S. Chand, M. C. Das, A water-stable twofold interpenetrating microporous MOF for selective $CO_2$ adsorption and separation, Inorg. Chem. 56 (2017) 13991-13997, https://doi.org/10.1021/acs.inorgchem.7b02136.
44. A. Pal, J.-B. Lin, S. Chand, M. C. Das, A 3D Microporous MOF with mab Topology for selective $CO_2$ adsorption and separation, ChemistrySelect 3, (2018) 917-921, https://doi.org/10.1002/slct.201702680.
45. S. Chand, A. Pal, M. C. Das, A moisture-stable 3D microporous $Co^{II}$-metal–organic framework with potential for highly selective $CO_2$ separation under ambient conditions, Chem. Eur. J. 24 (2018) 5982-5986, https://doi.org/10.1002/chem.201800693.
46. A. Pal, S. Chand, D. G. Madden, D. Franz, L. Ritter, A. Johnson, B. Space, T. Curtin, M. C. Das, A Microporous Co-MOF for highly selective $CO_2$ sorption in high loadings involving Aryl C–H···O═C═O interactions: combined simulation and breakthrough studies, Inorg. Chem. 58 (2019) 11553-11560, https://doi.org/10.1021/acs.inorgchem.9b01402.

47. S. Xiang, Y. He, Z. Zhang, H. Wu, W. Zhou, R. Krishna, B. Chen, Microporous metal-organic framework with potential for carbon dioxide capture at ambient conditions, Nat. Commun. 3 (2012) 954, https://doi.org/10.1038/ncomms1956.
48. C. Song, J. Hu, Y. Ling, Y. Feng, R. Krishna, D.-l. Chen, Y. He, The accessibility of nitrogen sites makes a difference in selective $CO_2$ adsorption of a family of isostructural metal–organic frameworks. J. Mater. Chem. A 3, (2015) 19417-19426, https://doi.org/10.1039/C5TA05481H.
49. K.-J. Chen, D. G. Madden, T. Pham, K. A. Forrest, A. Kumar, Q.-Y. Yang, W. Xue, B. Space, J. J. Perry IV, J.-P. Zhang, X.-M. Chen, M. J. Zaworotko, Tuning pore size in square-lattice coordination networks for size-selective sieving of $CO_2$, Angew. Chem. 55, (2016) 10268 –10272, https://doi.org/10.1002/anie.201603934.
50. R. Goswami, N. Seal, S. R. Dash, A. Tyagi, S. Neogi, Devising chemically robust and cationic Ni(II)–MOF with nitrogen-rich micropores for moisture-tolerant $CO_2$ capture: highly regenerative and ultrafast colorimetric sensor for TNP and multiple oxo–anions in water with theoretical revelation, ACS Appl. Mater. Interfaces 11 (2019) 40134-40150, https://doi.org/10.1021/acsami.9b15179.
51. N. Seal, M. Singh, S. Das, R. Goswami, B. Pathak, S. Neogi, Dual-functionalization actuated trimodal attribute in an ultra-robust MOF: exceptionally selective capture and effectual fixation of $CO_2$ with fast-responsive, nanomolar detection of assorted organo-contaminants in water. Mater. Chem. Front. 5 (2021) 979-994, https://doi.org/10.1039/D0QM00721H.
52. R.-B. Lin, D. Chen, Y.-Y. Lin, J.-P. Zhang, X.-M. Chen, A Zeolite-like zinc triazolate framework with high gas adsorption and separation performance, Inorg. Chem. 51 (2012) 9950- 9955, https://doi.org/10.1021/ic301463z.
53. J. D. Humby, O. Benson, G. L. Smith, S. P. Argent, I. da Silva, Y. Cheng, S. Rudić, P. Manuel, M. D. Frogley, G. Cinque, L. K. Saunders, I. J. Vitórica-Yrezábal, G. F. S. Whitehead, T. L. Easun, W. Lewis, A. J. Blake, A. J. Ramirez-Cuesta, S. Yang, M. Schröder, Chem. Sci. 10 (2019) 1098-1106, https://doi.org/10.1039/C8SC03622E.
54. C. Chen, W. Zhang, M. Zhang, J. Bai, Solvents-dependent formation of three MOFs from the $Fe_3O$ cluster and 3,3′,5,5′-diphenyltetracarboxylic acid and their selective $CO_2$ adsorption, Inorg. Chem. 58 (2019) 13836-13842, https://doi.org/10.1021/acs.inorgchem.9b01697.
55. D. Lv, R. Shi, Y. Chen, Y. Chen, H. Wu, X. Zhou, H. Xi, Z. Li, Q. Xia, Selective adsorptive separation of $CO_2/CH_4$ and $CO_2/N_2$ by a water resistant zirconium–porphyrin metal–organic framework, Ind. Eng. Chem. Res. 57, (2018) 12215-12224, https://doi.org/10.1021/acs.iecr.8b02596.
56. R. Maity, H. D. Singh, A. K. Yadav, D. Chakraborty, R. Vaidhyanathan, Water-stable adenine-based MOFs with polar pores for selective $CO_2$ capture, *Chem. Asian J.* **2019**, *14*, 3736-3741, https://doi.org/10.1002/asia.201901020.
57. J. Jia, Y. Wang, Y. Feng, G. Hu, J. Lin, Y. Huang, Y. Zhang, Z. Liu, C. Tang, C. Yu, Hierarchically porous boron nitride/HKUST-1 hybrid materials: synthesis, $CO_2$ adsorption capacity, and $CO_2/N_2$ and $CO_2/CH_4$ selectivity, *Ind. Eng. Chem. Res. 60*, (**2021**) 2463-2471, https://doi.org/10.1021/acs.iecr.0c05701.
58. D. Lv, J. Chen, K. Yang, H. Wu, Y. Chen, C. Duan, Y. Wu, J. Xiao, H. Xi, Z. Li, Q. Xia, Ultrahigh $CO_2/CH_4$ and $CO_2/N_2$ adsorption selectivities on a cost-effectively L-aspartic acid based metal-organic framework, Chem. Eng. J. *375*, (2019) 122074, https://doi.org/10.1016/j.cej.2019.122074.
59. N. Ni, Z. Chang, H. Huang, R. Feng, W. W. He, M. Zhong, D. G. Madden, M. J. Zaworotko, X.-He Bu, Specific $K^+$ binding sites as $CO_2$ traps in a porous MOF for

enhanced $CO_2$ selective sorption, Small 15 (2019) 1900426, https://doi.org/10.1002/smll.201900426.
60. J. D. Humby, O. Benson, G. L. Smith, S. P. Argent, I. da Silva, Y. Cheng, S. Rudić, P. Manuel, M. D. Frogley, G. Cinque, L. K. Saunders, I. J. Vitórica-Yrezábal, G. F. S. Whitehead, T. L. Easun, W. Lewis, A. J. Blake, A. J. Ramirez-Cuesta, S. Yang, M. Schröder, Chem. Sci. 10 (2019) 1098-1106, https://doi.org/10.1039/C8SC03622E.
61. O. T. Qazvini, S. G. Telfer, MUF-16: A robust metal−organic framework for pre-and post-combustion carbon dioxide capture, ACS Appl. Mater. Interfaces 13 (2021) 12141−12148, https://doi.org/10.1021/acsami.1c01156.
62. S. Nandi, S. Collins, D. Chakraborty, D. Banerjee, P. K. Thallapally, T. K. Woo, R. Vaidhyanathan, Ultralow parasitic energy for postcombustion $CO_2$ capture realized in a nickel Isonicotinate metal–organic framework with excellent moisture stability, J. Am. Chem. Soc. 139 (**2017**) 1734-1737, https://doi.org/10.1021/jacs.6b10455.
63. H.-M. Wen, G. Chang, B. Li, R.-B. Lin, T.-L. Hu, W. Zhou, B. Chen, Highly enhanced gas uptake and selectivity via incorporating methoxy groups into a microporous metal–organic framework, *Cryst. Growth Des.* 17 (2017) 2172, https://doi.org/10.1021/acs.cgd.7b00111.
64. H. Cui, Y. Ye, T. Liu, Z. A. Alothman, O. Alduhaish, R.-B. Lin, B. Chen, Isoreticular microporous metal−organic frameworks for carbon dioxide capture Inorg. Chem. 59 (**2020**) 17143, https://doi.org/10.1021/acs.inorgchem.0c02427.
65. L. Fan, S. Lin, X. Wang, L. Yue, T. Xu, Z. Jiang, Y. He, A Series of metal–organic framework isomers based on pyridine dicarboxylate ligands: diversified selective gas adsorption and the positional effect of methyl functionality, *Inorg. Chem.* 60 (**2021**) 2704, https://doi.org/10.1021/acs.inorgchem.0c03583.
66. Y. Chen, H. Wu, D. Lv, W. Yang, Z. Qiao, Z. Li, Q. Xia, An ultramicroporous nickel-based metal–organic framework for adsorption separation of $CO_2$ over $N_2$ or $CH_4$, Energy Fuels *32* (2018) 8676, https://doi.org/10.1021/acs.energyfuels.8b02287.
67. J. Jiang, Q. Wang, M. Zhang, J. Bai, A distorted $[Mn_2(COO)_4N_2]$ cluster based metal–organic framework with (3,3,6) topology and selective adsorption of $CO_2$, Cryst. Growth Des. 17 (2017) 2223, https://doi.org/10.1021/acs.cgd.7b00206.
68. X. Song, M. Zhang, J. Duan, J. Bai, Constructing and finely tuning the $CO_2$ traps of stable and various-pore-containing MOFs towards highly selective $CO_2$ capture, Chem. Commun. 55 (2019) 3477, https://doi.org/10.1039/C8CC10116G.
69. J.-R. Li, J. Yu, W. Lu, L.-B. Sun, J. Sculley, P. B. Balbuena, H.-C. Zhou, Porous materials with pre-designed single-molecule traps for $CO_2$ selective adsorption, Nat. Commun. 4 (2013) 1538, https://doi.org/10.1038/ncomms2552.
70. Y. Chen, D. Lv, J. Wu, J. Xiao, H. Xi, Q. Xia, Z. Li, Chem. A new MOF-505@GO composite with high selectivity for $CO_2/CH_4$ and $CO_2/N_2$ separation, Chem. Eng. J. 308,(2017) 1065, https://doi.org/10.1016/j.cej.2016.09.138.
71. M. J. Katz, Z. J. Brown, Y. J. Colón, P. W. Siu, K. A. Scheidt, R. Q. Snurr, J. T. Hupp, O. K. Farha, A facile synthesis of UiO-66, UiO-67 and their derivatives**,** Chem. Commun. 49 (**2013**) 9449, https://doi.org/10.1039/C3CC46105J.
72. J. An, S. J. Geib, N. L. Rosi, Cation-triggered drug release from a porous zinc−adeninate metal−organic framework, *J. Am. Chem. Soc.* 131 (**2009**) 8376, https://doi.org/10.1021/ja902972w.
73. Y. Pan, Y. Liu, G. Zeng, L. Zhao, Z. Lai, Rapid synthesis of zeolitic imidazolate framework-8 (ZIF-8) nanocrystals in an aqueous system, *Chem. Commun.* 47 (2011) 2071, https://doi.org/10.1039/C0CC05002D.
74. F. Luo, C. S. Yan, L. L. Dang, R. Krishna, W. Zhou, H. Wu, X. L. Dong, Y. Han, T.-L. Hu, M. O'Keeffe, L. L. Wang, M. B. Luo, R.-B. Lin, B. Chen, UTSA-74: A MOF-

74 Isomer with two accessible binding sites per metal center for highly selective gas separation, J. Am. Chem. Soc. 138 (**2016**) 5678, https://doi.org/10.1021/jacs.6b02030.
75. S. Xiang, W. Zhou, Z. Zhang, M. A. Green, Y. Liu, B. Chen, Open metal sites within isostructural metal–organic frameworks for differential recognition of acetylene and extraordinarily high acetylene storage capacity at room temperature Angew. Chem. Int. Ed. 49 (**2010**) 4615, https://doi.org/10.1002/ange.201000094.
76. K.-J. Chen, H. S. Scott, D. G. Madden, T. Pham, A. Kumar, A. Bajpai, M. Lusi, K. A. Forrest, B. Space, J. J. Perry IV, M. J. Zaworotko, Benchmark $C_2H_2/CO_2$ and $CO_2/C_2H_2$ separation by two closely related hybrid ultramicroporous materials, Chem 1(2016) 753, https://doi.org/10.1016/j.chempr.2016.10.009
77. P. Li, Y. He, Y. Zhao, L. Weng, H. Wang, R. Krishna, H. Wu, W. Zhou, M. O'Keeffe, Y. Han, B. Chen, A rod-packing microporous hydrogen-bonded organic framework for highly selective separation of $C_2H_2/CO_2$ at room temperature, Angew. Chem., Int. Ed. 54 (**2015**) 574, https://doi.org/10.1002/anie.201410077.
78. Y. Ye, Z. Ma, R.-B. Lin, R. Krishna, W. Zhou, Q. Lin, Z. Zhang, S. Xiang, B. Chen, Pore space partition within a metal–organic framework for highly efficient $C_2H_2/CO_2$ separation, J. Am. Chem. Soc. 141 (**2019**) 4130, https://doi.org/10.1021/jacs.9b00232.
79. H. Zeng, M. Xie, Y.-L. Huang, Y. Zhao, X.-J. Xie, J.-P. Bai, M.-Y. Wan, R. Krishna, W. Lu, D. Li, Induced fit of $C_2H_2$ in a flexible MOF through cooperative action of open metal sites, Angew. Chem., Int. Ed. 58 **(2019)** 8515, https://doi.org/10.1002/anie.201904160.
80. Z. Bao, D. Xie, G. Chang, H. Wu, L. Li, W. Zhou, H. Wang, Z. Zhang, H. Xing, Q. Yang, M. J. Zaworotko, Q. Ren, B. Chen, Fine tuning and specific binding sites with a porous hydrogen-bonded metal-complex framework for gas selective separations. J. Am. Chem. Soc. 140 (2018) 4596– 4603, https://doi.org/10.1021/jacs.7b13706.